JGR Solid Earth

RESEARCH ARTICLE
10.1029/2021JB022735

Special Section:
Ophiolites and Oceanic Lithosphere, with a focus on the Samail ophiolite in Oman

A Reference Section Through Fast-Spread Lower Oceanic Crust, Wadi Gideah, Samail Ophiolite (Sultanate of Oman): Petrography and Petrology

J. Koepke[1], D. Garbe-Schönberg[2], T. Müller[1], D. Mock[1], S. Müller[2], and S. Nasir[3]

[1]Institute of Mineralogy, Leibniz University Hannover, Hannover, Germany, [2]Institute of Geosciences, Kiel University, Kiel, Germany, [3]Department of Earth Sciences, Sultan Qaboos University, Muscat, Oman

Abstract In the absence of a complete profile through fast-spreading modern oceanic crust, we established a reference profile through the whole paleo crust of the Samail ophiolite (Sultanate of Oman), which is regarded as the best analogue for fast-spreading oceanic crust on land. To establish a coherent data set, we sampled the Wadi Gideah in the Wadi-Tayin massif from the mantle section up to the sheeted dikes and performed different analytical and structural investigations on the same suite of samples. This paper reports our studies of the lower crust, a 5 km thick pile of gabbros, focusing on petrographic features and on the results of mineral analyses. Depth profiles of mineral compositions combined with petrological modeling reveal insights into the mode of magmatic formation of fast-spreading lower oceanic crust, implying a hybrid accretion mechanism. The lower two thirds of the crust, mainly consisting of layered gabbros, formed via the injection of melt sills and in situ crystallization. Here, upward moving fractionated melts mixed with more primitive melts through melt replenishments, resulting in a slight but distinct upward differentiation trend. The upper third of the gabbroic crust is significantly more differentiated, in accord with a model of downward differentiation of a primitive parental melt originated from the axial melt lens located at the top of the gabbroic crust. Our hybrid model for crustal accretion requires a system to cool the deep crust, which was established by hydrothermal fault zones, initially formed on-axis at very high temperatures.

Plain Language Summary In this study we investigated the Samail ophiolite in the Sultanate Oman, which is best suited to deepen our understanding how the crust under oceans forms. This is possible, since "ophiolites" represents pieces of ancient oceanic crust and shallow mantle, injected into mountain chains long time ago, when former oceans were closed by tectonic forces. In the Wadi Gideah north of the town Ibra, we sampled a continuous profile through the lower crust consisting of gabbro, with the aim to understand the formation of the lower crust, which is up to now not well understood. The results of the analysis of the minerals in the gabbros and the careful study of the petrographic features observed in the gabbros, provide deep insights into the mechanism of the magmatic emplacement of the lower crust, implying a hybrid accretion mechanism. While the lower two thirds were formed by sill intrusions and *in situ* crystallization, the upper third of the gabbroic crust is dominated by downward differentiation of a primitive parental melt originated from the axial melt lens located at the top of the gabbroic crust.

Key Points:

- A reference profile through fast-spreading lower oceanic crust was established by outcrop sampling in the Wadi Gideah (Oman ophiolite)
- The results imply a hybrid accretion, with *in situ* crystallization in the lower and subsiding crystal mushes in the upper gabbroic crust
- Cooling of the deep crust was established by hydrothermal fault zones initially formed at very high temperatures in the magmatic regime

Supporting Information:

Supporting Information may be found in the online version of this article.

Correspondence to:

J. Koepke,
koepke@mineralogie.uni-hannover.de

Citation:

Koepke, J., Garbe-Schönberg, D., Müller, T., Mock, D., Müller, S., & Nasir, S. (2022). A reference section through fast-spread lower oceanic crust, Wadi Gideah, Samail ophiolite (Sultanate of Oman): Petrography and petrology. *Journal of Geophysical Research: Solid Earth*, *127*, e2021JB022735. https://doi.org/10.1029/2021JB022735

Received 9 JUL 2021
Accepted 8 DEC 2021

Author Contributions:

Conceptualization: J. Koepke, D. Garbe-Schönberg
Data curation: J. Koepke, T. Müller
Formal analysis: T. Müller, S. Müller
Funding acquisition: J. Koepke, D. Garbe-Schönberg, S. Nasir

1. Introduction

The formation and evolution of oceanic lithosphere by seafloor spreading at mid-ocean ridges is one of the dominant processes in the chemical differentiation and physical evolution of our planet. About two-thirds of the Earth's surface today was formed in this way. Lithosphere structure, architecture, properties, accretion, cooling, and alteration fundamentally differ between fast-spreading and slow-spreading systems. Oceanic crust formed at fast-spreading rates exhibits a relatively uniform seismic stratigraphy and is regarded as layered and relatively homogeneous (e.g., Canales et al., 2003). This is in contrast to oceanic crust generated at slow-spreading ridges which is characterized by considerable heterogeneity. There, crustal accretion is dominated by tectonic rather than solely by magmatic processes (e.g., Cannat, 1996; Dick et al., 2006). Theoretical models on magmatic accretion of the oceanic crust, thermal models, mass balance calculations for the whole ocean crust, or general alteration models only exist for fast-spreading systems. For slow-spreading systems, corresponding models and calculations are either not available, or not generally applicable. However, due to the lack of natural exposures or drill cores of the deep basement of fast-spreading oceanic crust, most models for fast-spreading crust have not

Investigation: J. Koepke, T. Müller, D. Mock, S. Nasir
Methodology: J. Koepke, D. Garbe-Schönberg, T. Müller, D. Mock, S. Müller
Project Administration: J. Koepke, S. Nasir
Resources: J. Koepke, S. Nasir
Software: S. Müller
Supervision: J. Koepke, D. Garbe-Schönberg
Validation: D. Garbe-Schönberg, D. Mock
Writing – original draft: J. Koepke
Writing – review & editing: J. Koepke, T. Müller, D. Mock, S. Müller, S. Nasir

been tested against natural samples to date (Christie et al., 2006; Teagle et al., 2012). Therefore, it is necessary to perform complementary studies on ophiolites, in particular on the Oman ophiolite, which is regarded as presenting the best example of fast-spreading oceanic crust on land, and which played a pivotal role in developing crucial paradigms for understanding sea floor spreading (e.g., Nicolas et al., 2000). The present study aims to perform a petrographical and petrological investigation of a complete crustal section in the Oman ophiolite, in order to establish a reference profile through fast-spreading oceanic crust. For this, a complete section, from mantle rocks to pillow basalts, was sampled at the Wadi Gideah in the Wadi Tayin massif of the Oman ophiolite during several field campaigns from 2010 to 2015. This profile is unique in terms of completeness of the crust-forming structural components and coherence and is well suited for a multi-methodological analytical approach in order to shed light on the accretion process of fast-spreading oceanic crust.

1.1. Crustal Accretion at Fast-Spreading Oceanic Ridges

Multi-channel seismic studies performed at the East Pacific Rise (EPR) revealed the presence of a lens filled with nearly pure melt in the mid-crust, often referred as the axial melt lens (AML; tens to hundreds of meters high, <2 km wide, sandwiched between the gabbro and the sheeted dike sequence). This is underlain by crystal/melt mush that is in turn laterally surrounded by a transition zone of mostly solidified material grading into a completely frozen zone, which corresponds to gabbros (e.g., Detrick et al., 1987; Vera et al., 1990). Together, the AML and the crystal mush beneath form the axial magma chamber. The role of the AML during crust accretion is still under debate. Either the AML is the source for the complete lower, gabbroic crust, formed by the suspension of crystal mush formed in the AML (the "gabbro glacier model," e.g., Henstock et al., 1993; Quick & Denlinger, 1993), or significant parts of the plutonic crust originate from in situ crystallization in the deep crust (the "sheeted sill model"; e.g., Bedard et al., 1988; Kelemen et al., 1997). However, most scientists believe that the magmatic processes responsible for magmatic accretion at fast-spreading oceanic crust are too complex to be explained with such simple end-member models, and that the truth probably lies somewhere in between these models (Boudier et al., 1996; Maclennan et al., 2004; Natland & Dick, 2009). Such hybrid models are also supported by the estimation of crystallization depths of MORB (Wanless & Shaw, 2012) and from recent multi-channel seismic studies indicating the presence of deep melt sills under recent fast/intermediate-spreading ridges (e.g., Canales et al., 2009; Carbotte et al., 2012, 2021; Marjanovic et al., 2014; Nedimovic et al., 2005).

The two end-member models mentioned above have profoundly different implications for the properties of the lower crust, including its composition (bulk rock geochemistry, composition and zoning of minerals), strain rate, cooling rate, hydrothermal fluid flux, fluid temperature, and intensity of high-temperature alteration. Long and coherent in-situ sections in the lower, plutonic crust of fast/intermediate-spreading mid-ocean ridges may allow the predicted variations of property signals to be compared with those from the natural rocks, offering the potential to shed significant light on the mode of accretion (see Figure 17 in Teagle et al., 2012). According to the "gabbro glacier" model, the differentiation of primitive MORB melts takes place in the AML below the sheeted dikes; thus, this model predicts a lower crust of more or less homogeneous composition, for example, gabbros which show a constant Mg# (MgO/(MgO + FeO) × 100, molar) both in the compositions of the bulk rocks, as well as in olivine and clinopyroxenes (from mineral core analyses). On the other hand, the "sheeted sill" model allows differentiation in the deep crust during ascent of the primitive MORB melt, predicting a higher bulk Mg# at the base of the crust and lower values with increasing crustal height (see Figure 5 in Maclennan et al., 2004). Results obtained so far in the lower fast-spreading oceanic crust are inconsistent. A profile sampled from outcrops in the Wadi Abyad in the Oman ophiolite revealed more or less constant Mg# with depth (MacLeod & Yaouancq, 2000), while International Ocean Discovery Project (IODP)drilling at Hess Deep at the EPR into the upper and lower gabbros revealed a zoned lower crust with evolved gabbros at the top and primitive gabbros at the base of the crust (Gillis, Snow, Klaus, & the Expedition 345 Scientists, 2014). The present study using a complete and coherent section through fast-spreading crust from the Oman ophiolite, with a high depth resolution (see below), helps to clarify these open questions.

1.2. Sections Through Modern Fast-Spreading Oceanic Crust

Away from transform faults, oceanic crust formed at fast spreading rates exhibits a uniform seismic stratigraphy and bathymetry, suggesting that fast-spreading oceanic crust is stratified and homogeneous. It is composed from top to bottom of basalts, sheeted dikes, gabbros, and peridotites. Consequently, our understanding of crustal

accretion processes and related geochemical cycles can be extrapolated to a significant portion of Earth's surface with some confidence. That said, the stimulus for having a reference section developed early on with the U.S. "MOHOLE" project in 1961 and culminated in submitting the "MISSON MOHO" proposal to IODP in 2007 (Christie et al., 2006; Ildefonse et al., 2009); to date this project has not been realized and, once started, it will take decades.

Past and present IODP drilling efforts into the basement of fast-spreading oceanic crust cover only the uppermost section or some deeper parts in areas that are strongly affected by ridge tectonism as outlined in the following. Previous IODP and Ocean Drilling Program (ODP) efforts to sample modern fast-spreading oceanic crust include Hole 504B on the southern flank of the Costa Rica Rift that penetrated 1.8 km into ~6.9 Ma Pacific Ocean igneous basement, but recovered only lavas and dikes (Alt et al., 1996). Drill hole 1256D in the basement of the Guatemala basin formed by the EPR ~15 Ma ago successfully cored a 1507 m long section of the upper (basaltic) oceanic crust, penetrating 76 m of the underlying gabbro sequence (Teagle et al., 2012; Wilson et al., 2006). In addition to these ODP and IODP drillings, two other prominent locations of fast-spreading oceanic crust are located at the EPR, where deeper crustal parts are exposed due to ridge tectonism: Hess Deep and Pito Deep. For Hess Deep, very short drill cores (decameters to max. ~150 m) of gabbro and mantle rocks were obtained by ODP and IODP. Here, for the first time in the basement of recent oceans, coherent series of primitive, "true" layered gabbro have been recovered, in a faulted area with an unknown crustal height (Gillis, Snow, Klaus, & the Expedition 345 Scientists, 2014). Geochemical analysis of these primitive lower plutonic rocks from the IODP drill cores, in combination with geochemical data for shallow-level gabbros drilled by ODP and basalts mostly recovered by dredging, provides the most completely constrained estimate of the bulk composition of fast-spreading oceanic crust so far.

In addition, ship-based *in situ* sampling was performed very locally as a function of depth, enabling the construction of "pseudo"-sections, both for Hess Deep (e.g., Lissenberg et al., 2013) and for Pito Deep (e.g., Brown et al., 2019; S. Maher et al., 2020; S. M. Maher et al., 2021) as summarized in Coogan (2014, and references therein). However, these "sections" cannot serve as a "reference" for deep fast-spreading oceanic crust for the following reasons: (a) data sets are highly incomplete; (b) possible faults related to ridge tectonics cause many problems; (c) it is not clear whether magmatism is representative, due to the special tectonic situation (propagating rifts); and (d) there is no upward stratigraphic continuation into the volcanic sequence. Consequently, a coherent “reference” profile through modern fast-spreading oceanic crust is still missing and will very probably not be obtained in the near future. This was the reason for the initiation of this study, to establish a reference profile in the Oman ophiolite, which can be in many aspects regarded as an analogue for modern EPR crust (as discussed in Section 4.1).

1.3. Previous Profiles Obtained in the Oman Ophiolite

As an alternative to sampling the modern oceanic crust, a reference profile through fast-spreading crust can be obtained by sampling an ophiolite section. However, most ophiolites either lack a coherent stratigraphy or are strongly influenced by a subduction-related setting. Thus, only the Oman ophiolite appears suitable for such an attempt based on results from previous studies performed in the last decades (e.g., Nicolas et al., 2000).

Initial work on the Oman ophiolite started with a U.S. mapping project performed in the late seventies. In the course of this project, a sample suite was collected through the entire ophiolite in the Ibra area of the Wadi Tayin massif. Samples were studied for some isotope systems (Gregory & Taylor, 1981; McCulloch et al., 1981) and for rare earth elements (REEs) (Pallister & Knight, 1981). In addition, a petrological profile based on mineral compositions was established (Pallister & Hopson, 1981), but only a few data were presented. Results obtained represented the state of the art at that time, for example, the evaluation of a model of km-thick chambers under the ridges filled with pure melt. The "ophiolite model" for the composition and structure of the oceanic crust was developed, and an early model for the alteration of oceanic crust via hydrothermal circulation was presented (Gregory & Taylor, 1981; McCulloch et al., 1981).

MacLeod and Yaouancq (2000) conventionally sampled the lower crust along the Wadi Abyad in the Nakhl-Rustaq block, revealing a 2,500 m long section through the plutonic crust. This profile includes earlier analytical results from rocks from the same section of Browning (1984). However, it is questioned whether this profile is really representative for the whole Oman ophiolite, since here the plutonic crust is relatively thin (2.5 km instead of 4 km

on average, Nicolas & Boudier, 2000), and, in addition, the gabbro sequence is, at least in part, strongly folded, which is unusual for the Oman ophiolite. A further disadvantage is a huge sample gap of ca. 400 m in the profile in the transition between the layered and the foliated gabbros.

Another important profile is located in the Wadi Khafifah, which runs parallel to the Wadi Gideah. The distance between both Wadis is only ca. 10 km, so that similarities are expected, when comparing these two profiles. The samples have originally sampled by P. Kelemen (Columbia University) at the end of the last century and have been used for several studies applying different analytical methods [cooling rates: Garrido et al. (2001) and VanTongeren et al. (2008); microstructures: VanTongeren et al. (2015)] A recent study from VanTongeren et al. (2021) focus on the accretion mechanism of the crust based on analytical work on bulk rocks and minerals. These authors defined a unit of "lower gabbros" where no systematic changes in composition with height was observed, and of “upper gabbros,” showing a marked increases in incompatible trace element concentration with crustal height. As accretion mechanism for the gabbroic crust these authors suggested the “Full Sheeted Sills” model, in which the whole gabbroic crust was emplaced by sill intrusions and in situ crystallization.

Some of the results of studies related to sections of the lower crust in the Oman ophiolite are summarized in Coogan (2014).

1.4. Geological Setting of the Oman Ophiolite

The Cretaceous Samail ophiolite in the Sultanate of Oman is regarded as the best example of fast-spreading oceanic crust exposed on land, and has been critically important in the development of crucial paradigms for understanding sea floor spreading and the formation of the oceanic crust (e.g., Nicolas et al., 2000). It presents sections of oceanic crust and the uppermost mantle beneath. The crustal sequence is complete and consists of, from the bottom to the top, the Moho transition zone (MTZ), layered gabbros, foliated gabbros, isotropic gabbros, sheeted dikes, and pillow basalts. A geological map can be found in Nicolas et al. (2000). Zircon dating revealed that the paleocrust was formed ∼95 Ma ago under fast-spreading conditions with a half-spreading rate of 50–100 mm/yr (Rioux et al., 2012, 2013).

Field relations and the results of geochemical and petrological studies suggest a polygenetic origin for the Oman ophiolite (e.g., Goodenough et al., 2014). A first phase produced the so-called V1 lavas and related gabbros that are very similar to the modern EPR crust in terms of structure, lithology, petrography, and bulk crustal thickness (Belgrano et al., 2019; Godard et al., 2003). However, in contrast to the EPR, the parental basaltic melts, which formed the crust during the first magmatic stage, show elevated water contents due to their formation in a subduction-influenced setting (Koepke, Feig, et al., 2021; MacLeod et al., 2013; Müller et al., 2017).

A second magmatic phase related to flux-induced peridotite melting, always intruding into the rocks of the first magmatic phase, shows characteristic lithologies like boninites in the upper crust, as well as wehrlites, gabbronorites, and larger plagiogranite bodies in the lower and mid-crust. The second, magmatic stage is much more voluminous in the northern blocks of the ophiolite (e.g., de Graaff et al., 2019; Goodenough et al., 2014; Juteau et al., 1988). Consequently, many studies focusing on understanding the crust accretion of mid-ocean ridges have been performed in the southernmost massif of the ophiolite, the Wadi Tayin massif, which is also the case for this study. During our field campaigns we did not find any wehrlite or gabbronorite bodies intruding the phase one gabbros, which are so common in the more northern massifs (e.g., 40% in the Haylayn massif, Juteau et al., 1988). Moreover, we did not find any larger (meter sized) plagiogranite in the gabbro outcrops of the mid-crust along the Wadi Gideah, only small plagiogranite vein and plug intrusions within the varitextured gabbro high up in the profile, which are interpreted as components of the AML (Müller et al., 2017). Concerning volcanics of the Phase 2 magmatism, we did not identify any boninite within our working area.

In spite of the inferred location of the ophiolite in a region of subduction zone initiation, the following observations related to the first magmatic phase demonstrate a close similarity with the modern, fast-spreading EPR: (a) a continuous layered crustal structure with a typical crustal thickness of ∼6 km, including a coherent plutonic section consisting of typical layered gabbros with a layering parallel to the crust/mantle boundary; (b) absence of typical “amagmatic” spreading that is common at slow-spreading ridges; (c) a very narrow range of zircon crystallization ages across the width of the ophiolite (max ∼ 100 km) sampled normal to the ridge direction; (d) spinel Cr/Al versus Mg# ratios that overlap those for peridotites from modern ridges; and (e) a well-developed sheeted dike sequence, orientated perpendicular to the Moho.

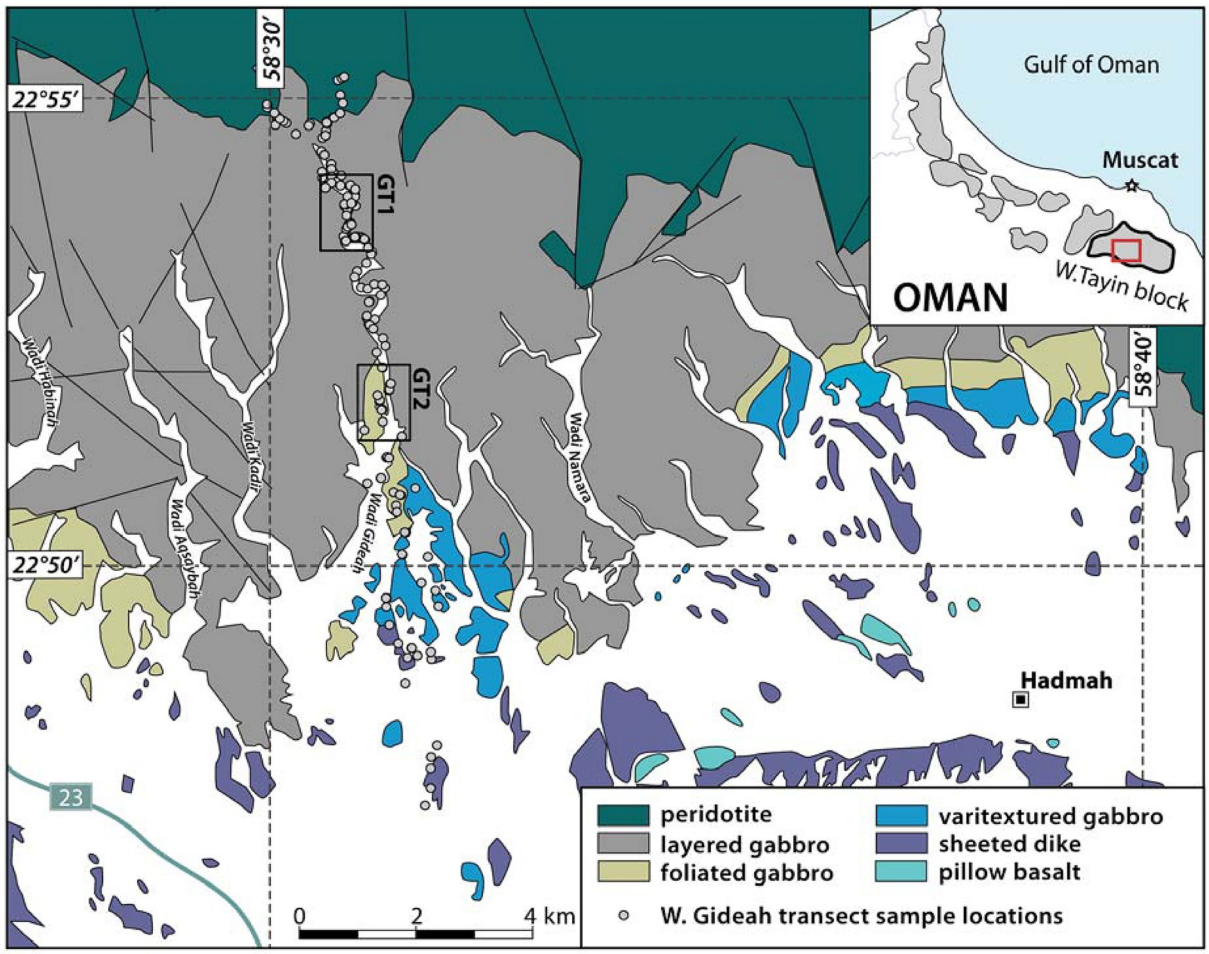

Figure 1. Geological map of the area north of Ibra within the Wadi Tayin massif of the Oman ophiolite showing the locations of the samples from the Wadi Gideah transect. The map is from Peters et al. (2005). The blank area defines quaternary sediments. Structural information, that is, the dips of structural features and a stratigraphic cross section through the Wadi Gideah, can be found in Pallister and Hopson (1981).

The southern massifs of the Oman ophiolite (Samail and Wadi Tayin block) are also the targets of the multi-national ICDP (International Continental Scientific Drilling Program) Oman Drilling Project (OmanDP, https://www.omandrilling.ac.uk/) which addresses a diverse range of scientific questions related to the formation, hydrothermal alteration, and biotic and abiotic weathering of oceanic lithosphere. The on-site activity in winter 2016/17 and 2017/18 produced nine wireline diamond cored boreholes and six air-rotary drilled boreholes. Two of the drill sites are located in the Wadi Gideah, where our reference profile presented in this study was sampled: GT1 dedicated to understanding deep layered gabbros within the deep crust (about 1 km above the crust/mantle boundary) and GT2 in the mid-crust for exploring the transition between the layered and the foliated gabbros (about 2.7 km above the crust/mantle boundary; see map in Figure 1). Thus, our ~5 km long reference section investigated in this paper, spanning the whole lower (plutonic) crust from the crust/mantle boundary to the dike/gabbro transition (DGT), is well suited to serve as a reference frame for the 400 m long drill cores recovered in the framework of the OmanDP. Due to a close cooperation with IODP, the scientific results of the OmanDP obtained so far are published under the umbrella of the IODP publishing platform (Kelemen et al., 2020).

2. Materials and Methods

2.1. Samples

The samples used for the reference profile project were collected from outcrops in the Wadi Gideah and surroundings during sampling campaigns in the years 2010, 2011, 2012, 2015, and 2016 (465 samples). For establishing a

profile through the whole crust in the Wadi Tayin block, we follow the approach of Pallister and Hopson (1981) based on an intensive U.S. mapping project in the 1970s where a few profiles from the Khafifah, Kadir, Gideah, and Imrad wadis have been described.

In order to construct a coherent profile, for this study we exclusively used samples from the Wadi Gideah (Figure 1), starting within the mantle section and ending in the sheeted dike sequence (no pillow basalts exist in this Wadi). The whole sample set for the Wadi Gideah reference profile comprises 293 samples, from which 274 thin sections were prepared. In many outcrops we collected more than one sample (up to 26 samples from two locations; see Table S1 in Supporting Information S1, PANGAEA data repository; Koepke, Garbe-Schönberg, et al., 2021), and we prepared more than one thin section from many rocks, which meant that we had identical crustal heights for many samples or thin sections (for calculation of the crustal height, see below). We collected from many locations several samples for different purposes (e.g., fresh samples for interpreting the primary magmatism; altered samples for the evaluation of the alteration grade and intensity; hornblende-bearing rocks produced by high-temperature hydrothermal activity). Therefore, averages or medians of such sample locations for specific downhole plots, where the properties of samples derived by thin section examination were plotted against crustal depth, would not represent the typical rock for a given crustal height. Moreover, standard deviations would be so large, that such points in the profile would be misleading and/or meaningless. Therefore, for the downhole plots for petrographic features derived by thin section investigations, we chose from such locations one representative thin section, resulting in 121 samples for the whole crustal height. With a crustal height of 5,009 m in total, this reveals an average sample per height resolution of 41 m.

We performed different analytical and structural investigations on the same suite of samples (pool sample concept). In this paper, we focus on the description of the lithologies of our transect, the petrographic characterization, and the presentation of the results of the phase analyses using an electron microprobe. One paper related to the crystallographic preferred orientations is already published in this volume (Mock, Ildefonse, et al., 2021). Other papers are currently in progress and will be published individually; crystallization temperatures estimated by the REE-in-clinopyroxene/plagioclase geothermometer (this volume), and bulk rock geochemistry (this volume). Samples and powders are available, and we welcome other applications for future studies focusing on further analytical and physical methods.

2.2. Calculation of Tilt Adjustment, Lithology Thicknesses, and Sample Depths

The Oman ophiolite was tilted during its obduction onto the continental crust of the Arabian Peninsula; therefore, sample field coordinates must be recalculated in order to obtain representative crustal thickness and valid sample heights within the Wadi Gideah reference profile. For this, we followed Pallister and Hopson (1981). GPS coordinates obtained in the field were transformed to the UTM system in order to simplify adjustment calculations. Then, sample coordinates in the UTM system were shifted to a fixed N-S axis by changing all x-coordinates to a single fixed value. The first appearance of true mantle rocks (typical harzburgite with porphyroclastic texture) was defined as the mantle/crust boundary. Referring to this location, for all sample coordinates the "Height above Mantle/Crust Boundary" (H.a.M.) was calculated using the UTM y coordinate and the equation

$$\text{H.a.M.}_{\text{sample}} = \text{UTM } y_{\text{sample}} - \text{UTM } y_{\text{Moho}}$$

The next step was to correct the H.a.M. value for the general tilt of the Wadi Gideah area, using the equation

$$\text{H.a.M. final}_{\text{sample}} = \text{H.a.M.}_{\text{sample}} \times \sin(\alpha)$$

As dip angle α we used the average of dip angles measured in the field by Pallister and Hopson (1981) for the whole Wadi Gideah area ($\alpha = 28°$). The pronounced syncline structure in the south of Wadi Gideah (see Figure 2 in Pallister & Hopson, 1981) was not taken into account, in order to simplify the calculation of the H.a.M. However, we stopped this calculation procedure at a crustal height of 5,009 m within the DGT, in an area where the last coherent outcrops of varitextured gabbro in the Wadi bed descend below the Ibra plain. Further south only small and insignificant hills of exclusively sheeted dike basalts overtopped the Ibra plain, for which consequently no H.a.M. value was calculated. The H.a.M. values of all samples are summarized in Table S1 in Supporting Information S1 (PANGAEA data repository; Koepke, Garbe-Schönberg, et al., 2021). The altitudes of the samples were not taken into account, since samples were generally taken from the Wadi bed.

2.3. Petrography

For the definitions of rock names, and for terms used in the petrographic characterization (e.g., grain size rank) obtained by thin sections, we followed the IODP rules for typical gabbro legs (Gillis, Snow, Klaus, Abe, et al., 2014). Modes were estimated using mode estimation charts. The results of the thin section descriptions, including the coordinates and what structural unit each sample is assigned to, are summarized in Table S1 in Supporting Information S1 (PANGAEA data repository; Koepke, Garbe-Schönberg, et al., 2021). For most samples this table presents detailed petrographic descriptions of rocks and minerals. However, due to the high number of petrographically investigated thin sections, for some samples only the characterization of the rocks without details of the minerals are given. This table contains the petrographic characterization of 230 samples based on 252 thin sections.

2.4. Phase Analyses by Electron Probe Microanalysis

The analyses of the mineral phases were performed with a Cameca SX100 electron microprobe equipped with five spectrometers and the "Peak sight" operating software. All data were obtained using 15 kV acceleration potential, a static (fixed) beam, Ka emission from all elements, and the "PAP" matrix correction by Pouchou and Pichoir (1991) using natural and synthetic standards. Most element concentrations were obtained with a beam current of 15 nA and a counting time of 10 s on peak and background. For F and Cl in amphibole and for Mg, Ti, and K in some plagioclases, we applied higher beam currents (40 nA) and increased counting times (60–120s) leading to more accurate trace element data and lower limits of detection, see Koepke et al. (2005).

For most samples we analyzed both cores and rims of the minerals. For an evaluation of the statistical significance of the differences in the concentrations between cores and rims, p-values were calculated based on a *t*-test. With respect to rim divided by core factors, only those p-values <0.05 were considered, leading to a significance level that a zoning is true of higher than 95%. This approach resulted in a significant reduction of analyzed rim/core values, as demonstrated for plagioclase; of 86 analyzed rim/core values, 53 passed the *t*-test and are regarded as statistically meaningful.

3. Results

3.1. Structural Units and Crustal Thickness

In order to assign the samples to structural units we used the following scheme (from bottom to top): MTZ, Layered Gabbro Unit, Foliated Gabbro Unit, DGT. We divided the Foliated Gabbro Unit into an upper (UFG) and a lower (LFG) unit, following Mock, Ildefonse, et al. (2021), who found different emplacement mechanisms for these two subunits, based on an interpretation of the microstructures evaluated from EBSD measurements applied to 68 samples out of our sample set. We will see in the following that this subdivision is also of significance with respect to the petrography and mineral chemistry investigated in this paper.

For the definition of the contacts between the units, their crustal heights, and for their thicknesses see Table 1. The thickness of the whole plutonic crust, including the DGT, is 5,009 m, which corresponds well to an average thickness of the plutonic crust of the Wadi Tayin area from Pallister and Hopson (1981; 5.0 km, based on four sections). Corresponding values from Nicolas and Boudier (2000) for the plutonic crust of the Wadi Tayin massif are, on average, a little bit smaller (3.7 ± 1.2 km, based on 12 sections). General uncertainties arise concerning the thickness of the DGT, which includes both dikes and gabbros (isotropic, varitextured), and it is not clear where the different authors made the distinction between the plutonic and the volcanic crust. When we assigned the top boundary of the plutonic crust to where the first basaltic dikes appear, our profile shows a thickness of 4.8 km, which is within the error of the estimations of Nicolas & Boudier, 2000. Using this value, and adding the average value for the total volcanic crust estimated by Nicolas & Boudier, 2000 of 1.7 km, we end up with a thickness of 6.5 km for the complete crust for the Wadi Gideah area. This value fits quite well with an average thickness of 6.8 km for the EPR crust, estimated by seismic studies (Canales et al., 2003).

Table 1
Crustal Units Within the Wadi Gideah Reference Profile

Crustal Unit		Upper contact (H.A.M., meter)	Definition of the upper contact	Definition of the lower contact	Unit thickness (meter)
Dike/gabbro transition		5,009	100% basalts	lowermost varitextured gabbros	727
Foliated gabbro	Upper Foliated Gabbro	4,282	lowermost varitextured gabbro	from Mock et al. (2021) based on EBSD results	757
	Lower Foliated Gabbro	3,525	from Mock et al. (2021) based on EBSD results	lowermost foliated gabbros	877
Layered gabbro		2648	lowermost foliated gabbro	uppermost cumulate dunite	2488
Moho transition zone		159	uppermost cumulate dunite	occurence of mantle tectonite	159
Total					5,009

3.2. Field Relations

3.2.1. Moho Transition Zone

Our profile starts in the mantle section of the most northern part of our working area (Figure 1), which consists of harzburgites with typical porphyroclastic textures, recording typical mantle flow. Heading to the south, the occurrence of the first coherent cumulate rocks marks the start of the MTZ; these rocks consist of olivine gabbros, cumulate dunites, troctolites, anorthosites, and wehrlites (Figures 2g and 2h), with a thickness of ∼160 m. All these cumulate rocks show a coherent layering, with planar contacts, and with layering and foliation sub-parallel to the Moho, transitioning to the layered gabbro unit above without any discontinuity. Massive dunites always form coherent layers (Figure 2h), up to a thickness of decameters for an individual layer, very similar to the observations within the OmanDP drill cores CM1 and CM2 which penetrated the MTZ in the Wadi Zeeb (Kelemen et al., 2020). These sites are also located within the Wadi Tayin massif, about 20 km west of Wadi Gideah. The same is true for wehrlites; in our sample collection, with one exception, they are found within the MTZ. As in the CM1 and CM2 OmanDP drill cores (Kelemen et al., 2020), the wehrlites form coherent layers on the cm to dm scale (Figure 2g). Crosscutting wehrlites, as reported by Nicolas and Boudier (2000) to be typical for the MTZ in Oman, have not been observed in the Wadi Gideah.

3.2.2. Layered Gabbros

The absence of cumulate dunite marks the start of the Layered Gabbros Unit, which is typically composed of foliated olivine gabbros showing a marked layering, including olivine-bearing gabbro, rare troctolites, and olivine-free gabbros. This unit is ∼2,490 m thick, with layering and foliation sub-parallel to the Moho, and planar contacts. These rocks often show a typical modal layering on the cm to dm scale, where darker (olivine-rich) and lighter (plagioclase-rich) layers alternate (Figure 2c); olivine abundances gradually decrease from layer bases to tops. The observed features are very similar to those in the layered gabbros described by Mock et al. (2020) in Wadi Somerah (Sumail block); they suggested as a formation mechanism that the layers were deposited by density currents of crystal-laden magma within a sill environment. Much more abundant within the Layered Gabbro Unit are gabbros showing cryptic layering, where the establishment of a stratiform layering is not visible. Very rare are outcrops characterized by a fine lamination on the mm scale (Figure 2d). This type of layering is very similar to that described by Mock et al., 2020, from the Wadi Wariyah (Sumail block); the authors suggest "Ostwald ripening" as the layer formation mechanism. Very rare are outcrops where shear zones can be observed which were formed at very high temperatures. No plastic deformation was observed, implying that the shearing proceeded in the magmatic regime, with a small, but distinct amount of melt always present (see details in Figure 2e). In the lowermost Layered Gabbro Unit close to the MTZ, special troctolites can be found, consisting of a troctolitic, strongly foliated matrix which includes cm-sized oikocrysts of clinopyroxene (Figure 2f). Such "oikocryst troctolites" are well known from the lowermost gabbro drilled by IODP in Hess Deep at the EPR (Gillis, Snow, Klaus, & the Expedition 345 Scientists, 2014).

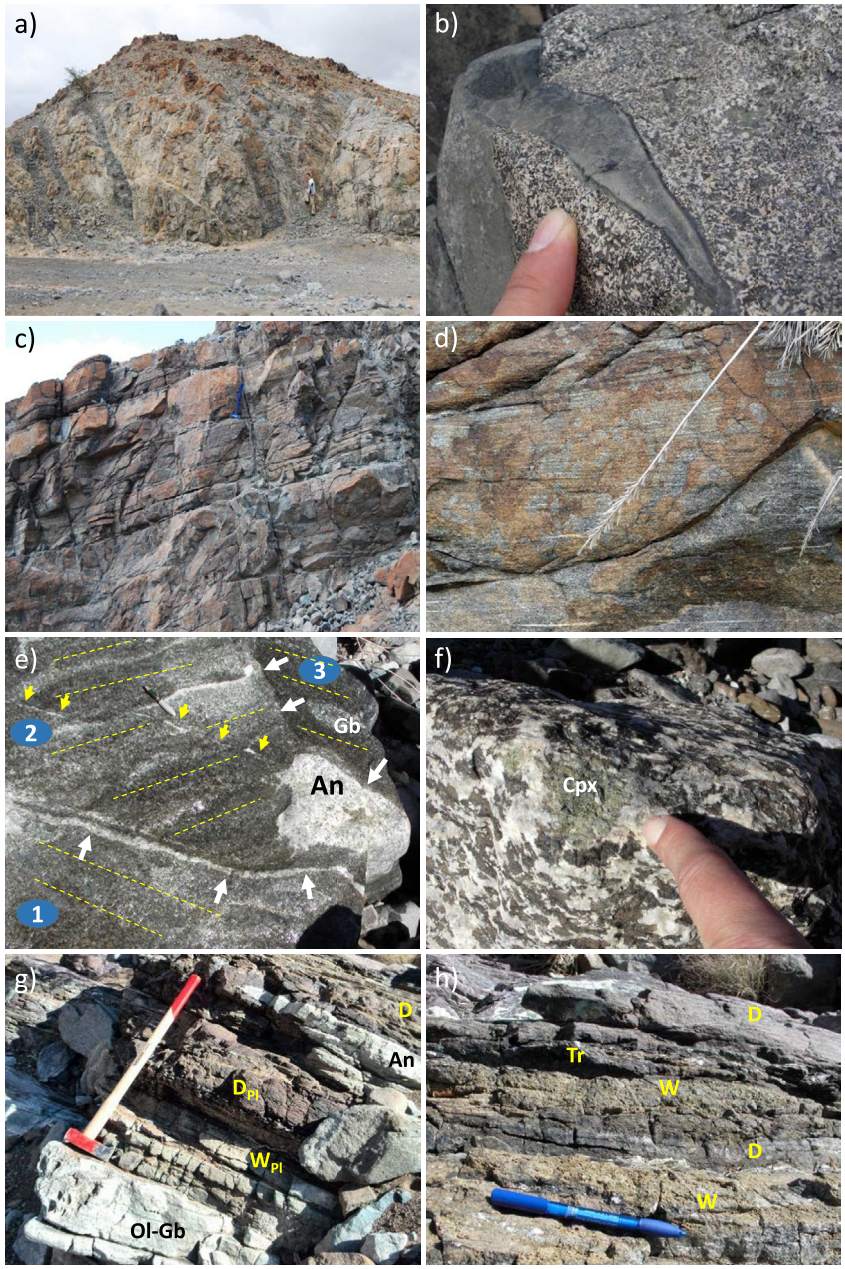

Figure 2.

3.2.3. Foliated Gabbros

At ~2,650 m H.a.M, the appearance of the first foliated gabbro within the series of monotonous layered gabbro marks the lower boundary of the unit of "foliated gabbros". These are olivine gabbros, olivine bearing, and olivine free gabbros with foliation, often associated with typical late stage minerals like brown hornblende, orthopyroxene, and Fe-Ti oxide, which are not known from the Layered Gabbro Unit. The foliated gabbros show a typical lineation and significantly smaller grain size than the layered gabbros. The transition between layered and foliated gabbros is marked by a ~100 m thick zone, where sequences of both typical layered gabbros with coherent layering (Figure 2c) as well as fine grained foliated gabbros with typical lineation and without any sign of layering occur. Upsection, the dip of the foliation steepens, as described within this unit at many locations within the whole ophiolite (e.g., in the Haylan block, MacLeod & Yaouancq, 2000). The whole foliated gabbros unit is ~1630 m thick. In the field, we did not record a difference between the foliated gabbros in the LFG and

in the UFG. But, a significant differences are manifested in the petrographic features (especially in the mineral mode; see Section 3.3) and in the mineral compositions (see Section 3.4).

3.2.4. Dike/Gabbro Transition

At ~4,280 m H.a.M., the first so-called varitextured gabbro appears, marking the start of the transition between the foliated gabbro and the DGT. The uppermost unit of the Wadi Gideah profile is the ~730 m thick DGT, consisting mainly of isotropic, often hornblende- and Fe-Ti oxide-bearing gabbros with patchy appearance, called "varitextured" due to the strong heterogeneities in texture. This term was introduced for typical gabbros found in the Oman ophiolite between the sequence of foliated gabbros and the sheeted dikes, also known as "high-level," "isotropic," or "upper" gabbro (e.g., MacLeod & Yaouancq, 2000; Pallister & Hopson, 1981). This unit also contains some felsic rocks often named (oceanic) plagiogranites (quartz diorites, tonalites, trondhjemites), which are volumetrically insignificant in the Wadi Gideah area. Often, the varitextured gabbros cut formerly emplaced dikes (basalts or dolerites) or are cut by basaltic dikes (Figure 2b). Foliated gabbros also occur in the lower part of this unit, with unclear intrusion relationships with the varitextured gabbros, due to the lack of suitable exposures. Varitextured gabbros are only known from fast-spreading ridges (see review in Koepke & Zhang, 2021), and are regarded as the frozen fillings of the AML, formed by in-situ crystallization. The DGT unit ends at the southern margin of our working area, where no more isotropic gabbros occur. The last gabbro outcrop represents a spectacular rock association of varitextured gabbro, cut by massif quartz diorites and tonalites, which are in turn cut by later trondhjemite dikes, which are finally cut by basaltic dikes (Figure 2a). Outcrop details, intrusion relations, as well as petrography and geochemistry of these rocks are presented in Müller et al. (2017).

3.2.5. Hydrothermal Fault Zones

The crustal units are cut by dozens of hydrothermal fault zones (HTFZs), which are characterized by pervasive alteration, mainly in greenschist and sub-greenschist facies. Mostly, these zones are decameters thick (Figure 3a), but some are smaller, on the scale of meters, and some are several hundred meters wide. Typical outcrops show whitish colors (Figure 3a), so they can be identified from far away, even in aerial photographs. Samples from here are brittle and highly altered, sometimes completely converted to so-called metagabbros, consisting of typical greenschist-facies minerals like chlorite, actinolite, epidote, serpentine, albite, and prehnite. Depending on the outcrop conditions, discrete fault zones can be observed cutting the layering in the layered gabbros with a steep dip (Figure 3b).

Figure 2. Photographs of outcrops from principal units of the lower crust in the Wadi Gideah. For details see text. (a) Dike/Gabbro Transition (DGT): Southernmost outcrop in the Wadi Gideah before reaching the Ibra plain, frozen melt lens at the transition between gabbro and dike, consisting of varitextured gabbro, quartz diorite, tonalite, and trondhjemite with complex intrusion relationships, cut by parallel oriented basaltic dikes. For details of this outcrop see Müller et al. (2017). N22.819°, S58.527°, H.a.M = 5009 m. (b) DGT: Basaltic dike with chilled margins cuts varitextured gabbro as a characteristic feature of the DGT in the lower Wadi Gideah. N22.828°, S58.523°, H.a.M = 4547 m. (c) Outcrop showing typical cm- to dm-scale modal layering with planar contacts, as is typical for the layered gabbro unit. Darker olivine-rich layers alternate with whitish plagioclase-rich layers. This outcrop is from a small side valley of the Wadi Gideah main valley. N22.894° E58.535°, H.a.M = 1072 m. (d) Layered Gabbro Unit: Outcrop in the deeper layered gabbro characterized by a fine lamination on the mm scale. Maximal thickness is shown by white, anorthositic layers with a thickness of about 1 cm. This type of layering is very rare in the Wadi Gideah. It is very similar to the type of layering described by Mock et al. (2020) from the Wadi Wariyah. Here, the mm layering is best explained by Ostwald ripening. N22.8936°, S58.5152°, H.a.M = 1114 m. (e) Layered Gabbro Unit: Outcrop in the deeper layered gabbro showing the complex relationships between three blocks of mainly olivine gabbro (numbered), which are separated from each other by shear zones (white arrows). Layering is diffuse, but still clearly visible. Each block shows a different layering orientation, marked by the yellow dashed lines. While the shear zone that developed between blocks 1 and 2 is diffuse, exhibiting a composite band of a leucocratic and a mafic gabbro parallel to the shear zones, the shear zone between blocks 2 and 3 is sharp without any discontinuity. Block 2 shows internal shear zones (marked by yellow arrows) filled with anorthositic gabbro, which offset the layering. Block 2 contains an irregularly formed, dm-sized domain of anorthosite (An), representing a "block within a block." The contact between the anorthosite and the host gabbro is diffuse, irregular, and sutured. In contrast, the contact between the anorthosite and block 3 is sharp, due to the influence of the shear zone. Block 3 also contains a small block composed of gabbro (Gb) with diffuse, sutured contacts, which is lens shaped and aligned with the foliation induced by the layer-forming process. Note that no plastic deformation was observed, implying that the shearing proceeded in the magmatic regime, with a small, but distinct amount of melt always present. N22.8920° E58.5144°, H.a.M = 1205 m. (f) Layered Gabbro Unit: Outcrop in the lowermost Layered Gabbro Unit close to the Moho transition zone (MTZ), showing troctolite which includes a cm-sized oikocryst of clinopyroxene (Cpx). While the troctolite shows a marked foliation with parallel-orientated olivines and plagioclase, the plagioclase chadacrysts within the clinopyroxene do not show any preferred orientation. Such features are well known from the lowermost gabbro drilled by International Ocean Discovery Project (IODP) at Hess Deep at the EPR (Gillis, Snow, Klaus, & the Expedition 345 Scientists, 2014). N22.910°, S58.511°, H.a.M = 272. (g) MTZ: Sequence of alternating layers with planar contacts of (from top to bottom) dunite (D), anorthosite (An), plagioclase-bearing dunite (DPl), plagioclase-bearing Wehrlite (WPl), and olivine gabbro (Ol-Gb). Length of the sledge hammer is 90 cm. N22.913°, S58.502°, H.a.M = 119 m. (h) MTZ: Alternating cm-thick layers of dunite (D), troctolite (Tr), and wehrlite (W), which is a typical sequence for the MTZ. N22.913°, S58.502°, H.a.M = 119 m.

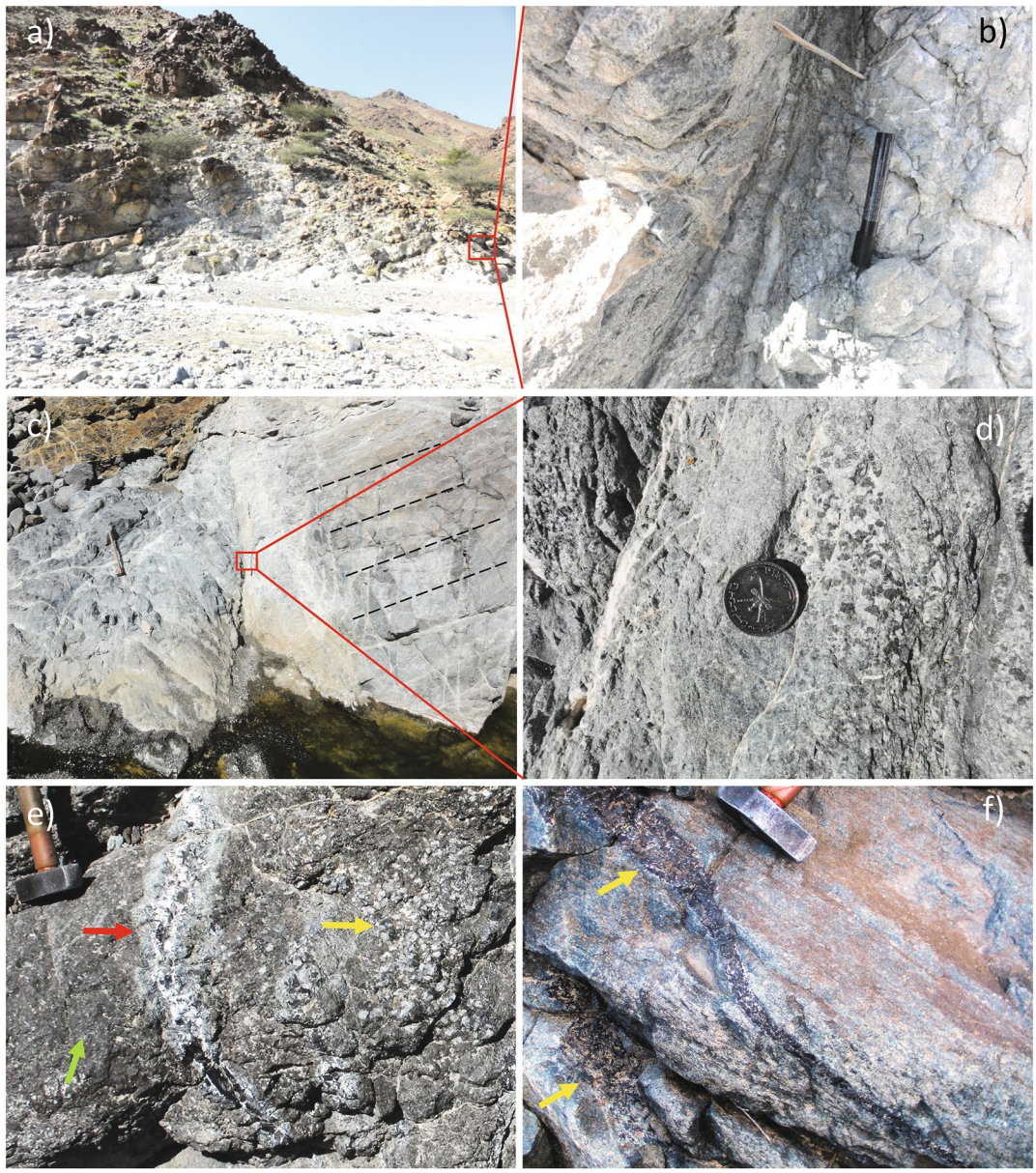

Figure 3. Photographs of outcrops from Hydrothermal Fault Zones (HTFZs) cutting layered gabbros within the lower crust in the Wadi Gideah. For details see text. Description of samples related to these outcrops can be found in Table S1 in Supporting Information S1 (PANGAEA data repository; Koepke, Garbe-Schönberg, et al., 2021). (a) Typical appearance of an HTFZ in the field showing grayish, whitish colors. Samples from here are brittle and highly altered, with former layered gabbros often converted to metagabbros. Sample OM12-50 originated here, an isotropic hornblende disseminated oxide gabbro. N22.878°, S58.519°, H.a.M = 1934 m. (b) Detail from (a): marked rectangle. Visible is a fault zone cutting steeply through highly altered layered gabbro, now metagabbro consisting of alteration phases, sometimes with relics from the magmatic stage. (c–e) Special multiple HTFZs at H.a.M. from 1205 m to 1237; for details see text. (c) Layered gabbro cut by a steeply dipping HTFZ. Layering is indicated by dashed lines. Several samples originated here including OM12-Hy55B (brown material upper left); OM12-Hy58.5 and OM12-Hy59 (area where the hammer is located); OM12-Hy59.5 (marked with a red rectangle); and OM12-Hy62 (right of the marked rectangle in the right part of the outcrop with the dashed lines). N22.892°, S58.517°, H.a.M = 1205 m. (d) Details from (c), showing within the fault gouge a clast of a formerly medium-grained isotropic hornblende gabbro, now strongly altered to metagabbro (sample OM12-Hy59.5). (e) Complex intrusion relations: layered gabbro (not visible) is cut by an isotropic, very heterogeneous gabbro consisting of very coarse-grained hornblende gabbro (yellow arrow, OM12-Hy032B) associated with a medium-grained "wehrlitic" hornblende gabbro (green arrow, sample OM12-Hy032A), cut by a magmatic vein of pegmatitic hornblende gabbro with prismatic hornblende up to 10 cm long (red arrow, sample OM12-Hy032C). N22.892°, S58.517°, H.a.M = 1205 m. (f) Layered olivine gabbro in the Moho transition zone cut by hornblende diorite veins. Some meters away, the diorite vein propagates into a pure hornblende vein. The samples OM15-19A, B, and C originate here. N22.915° E58.500°, H.a.M = 16 m.

Since we focused in this study on primary magmatic features, we did not perform a sophisticated geological mapping of all HTFZs, but we sampled many of these (22 locations mainly in the Layered Gabbro Unit). Thus, the sampling was incomplete, but allows us to characterize petrographic features and to draw petrologic conclusions. Samples taken in HTFZ outcrops are marked in Table S1 in Supporting Information S1 (PANGAEA data repository; Koepke, Garbe-Schönberg, et al., 2021), and sample descriptions can also be found there. These zones are distributed over the whole transect with a significantly higher density upsection. We stopped the systematic sampling of these zones at an H.a.M. of 2,915 m, in a horizon where the first foliated gabbros occur. Thus, the absence from our sample suite of HTFZ rocks higher than 2,915 m does not mean that no more of these zones exist. Above, these zones are much larger (several hundred meters wide) and much more diffuse, preventing focused sampling. We identified several of these "cooked areas", for example, at the OmanDP drill site GT2 (H.a.M. = 2,695), in the upper foliated gabbros at H.a.M. = 3,589 m, and within the DGT unit at H.a.M. = 4,600 m.

At H.a.M. = 1092 m, one HTFZ occurs within the Layered Gabbro Unit, which is described in detail by Zihlmann et al. (2018), with focus on the petrology of the fault rocks, whole rock mass change calculations, and isotope work. This study shows that these zones can be interpreted as pathways for focused hydrothermal flow, in accord with Coogan et al. (2006), who investigated such zones in Wadis some kilometers east of the Wadi Gideah.

One important observation is that in the central areas of many of these zones, we observed the occurrence of characteristic rocks, mostly isotropic coarse grained hornblende gabbro, sometimes with pegmatitic grain sizes (Figure 3e), which cut the layered gabbro, mostly with a steep dip. It is important to note that none of these hornblende-bearing rocks is observed as part of the "normal" layered gabbros. Another observation is that in these zones mm-to cm-thick veins of hornblende diorite occur (Figure 3f), which sometimes develop to pure brown hornblende veins. In addition, in many of these zones we observed the formation of magmatic hornblende in the adjacent host gabbros. We discuss the implications of these observations in Section 4.6.

At H.a.M. from 1205 to 1237 m, a ~250 m wide HTFZ exists, which shows multiple zones cutting steeply layered gabbro. In contrast to other HTFZs, here the pervasive alteration into greenschist facies is less pronounced. Therefore, this zone gives us insight into the initial formation state of a HTFZ, where hydrous fluids interacted with frozen rocks at very high temperatures. Most rock samples from this zone have a special sample name code, with the prefix OM12-followed by "Hy" and a number, which corresponds to meter, with "0" (m) at the western starting point and "166" (m) in the more eastern part of this zone. It ends with sample OM12-027. For details of these samples see Table S1 in Supporting Information S1 (PANGAEA data repository; Koepke, Garbe-Schönberg, et al., 2021). Since here the Wadi follows more or less the east-west direction, samples taken here show a similar calculated height (see Section 2.2 for calculation of the crustal height); thus this part of the Wadi corresponds more to a profile of lateral variation than of crustal height. Some highlights of this peculiar HTFZ are presented in the following.

1. Complex intrusion relations at 32 m (starting from "0" m at the western border). Here, layered gabbro is cut by an isotropic, very heterogeneous gabbro consisting of very coarse-grained hornblende gabbro, associated with a medium-grained "wehrlitic" hornblende gabbro; these are in turn cut by dm-thick magmatic veins of pegmatitic hornblende gabbro with prismatic hornblende up to 10 cm long. For details and sample names see Figure 3e.
2. Layered gabbro cut by a steeply dipping shear zone and by wehrlitic gabbro from 54 to 63 m. Here, relatively fresh layered gabbro occurs with layering still visible, which is cut by a steeply dipping high temperature shear zone (Figure 3c). Within the fault gouge, cm-sized clasts of a former medium-grained isotropic hornblende gabbro exist; this gabbro has been strongly altered to metagabbro (Figure 3d). In addition, at this location, the layered gabbro is cut by a coarse-grained brownish wehrlitic gabbro (Figure 3c). For details and sample names see Figures 3c and 3d.
3. Within this special HTFZ are countless mm- to cm-sized magmatic veins of hornblende-bearing diorites cutting the layered gabbro mostly with steep dip. The vein diorite is quite evolved, bearing brown hornblende, orthopyroxene, and apatite (see Section 3.3.2). Since the layered gabbro hosting these veins is in many places relatively fresh, the corresponding samples provide insight into details of the underlying reactions between hydrothermal fluids and solid gabbro, at the transition between the metamorphic and magmatic regime. We focus on that in Section 3.3.2.

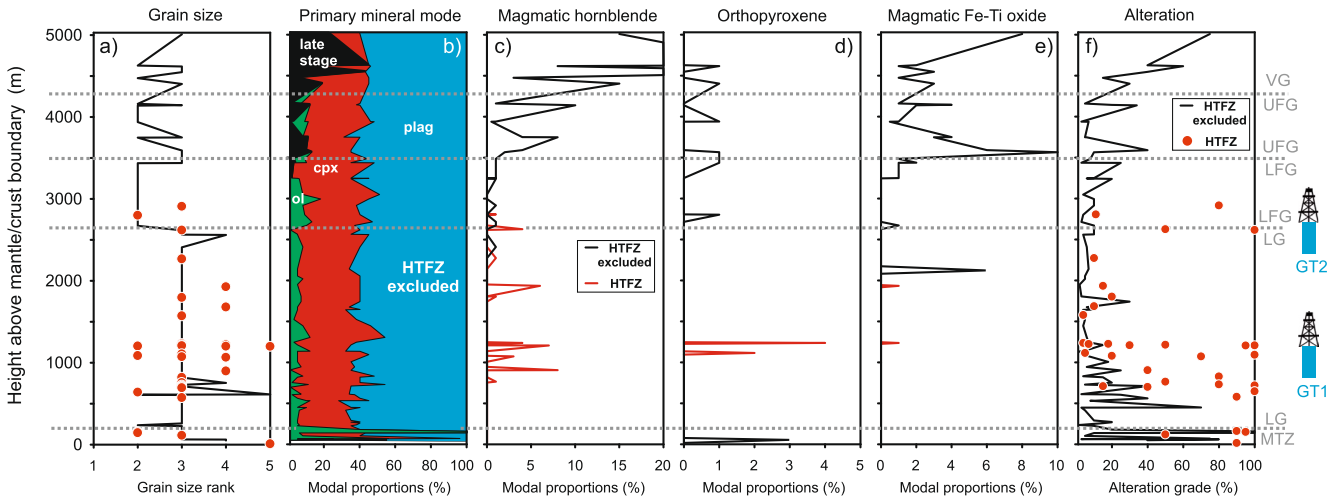

Figure 4. Plots for various parameters against crustal height obtained from Table S1 (PANGAEA data repository; Koepke, Garbe-Schönberg, et al., 2021). If more than one rock was sampled at a given crustal height, only one representative sample was selected. Included are the GT1 and GT2 locations of the OmanDP (length of the cores = 400 m), as well as the boundaries between the crustal units (MTZ–Moho transition zone, LG–Layered Gabbro Unit, LFG–Lower Foliated Gabbros, UFG–Upper Foliated Gabbros, VG–varitextured gabbro of the DGT). For details see text. (a) Grain size rank for rocks with and without a visible record of a hydrothermal fault zone (HTFZ). For legend see f). Values: 1—microcrystalline (0.1–0.2 mm); 2—fine grained (0.2–1 mm); 3—medium grained (1–2 mm); 4coarse grained (2–5 mm); 5—very coarse grained (>5 mm). (b) Mode of the primary minerals. Samples showing an influence of HTFZ are excluded. Late stage minerals comprise magmatic hornblende, orthopyroxene, and Fe-Ti oxide. (c–e) Modal proportions of magmatic hornblende, orthopyroxene, and magmatic Fe-Ti oxide, respectively, for rocks with and without an HTFZ record. For legend see (c). (f) Grade of alteration for samples with and without an HTFZ record.

HTFZs can be observed in the whole layered gabbro unit, and even below in the MTZ. In the ~160 m thick MTZ we sampled three such zones. The lowest HTFZ at 16 m height above the Moho shows spectacular multiple cm-thick hornblende diorite veins crosscutting layered gabbro (Figure 3f). Some of these veins propagate into a pure hornblende vein.

3.3. Petrography

It is important to note that we followed a strict protocol, characterizing the rocks related to an HTFZ process separately from those not influenced. This is necessary, since many variations in terms of mineral composition, mode, and grain size can be attributed to the influence of an HTFZ. This is obvious from diagrams created using data obtained from thin sections versus crustal height (Figure 4); rocks with and without HTFZ influence are plotted separately, showing different behavior. Petrographic parameters used in the plots for the latter group are restricted to (secondary) formations in the magmatic regime; metamorphic rocks or metagabbros are not considered here. Petrographic details of all samples, including modes, structures, textures, grain sizes, and grade of alteration can be found in Table S1 in Supporting Information S1 (PANGAEA data repository; Koepke, Garbe-Schönberg, et al., 2021).

In Figure 4a the grain size rank clearly shows the sharp boundary between the Layered Gabbro Unit and the foliated gabbros, making it very easy to distinguish between these types of gabbro. This figure also shows the "noise" produced by those rocks which are influenced by an HTFZ in their formation. The primary mineral mode is shown in Figure 4b. For clarity we lumped the modal amounts of interstitial late stage minerals together (hornblende, Fe-Ti oxide, orthopyroxene). These start to appear in general at the LFG/UFG boundary, emphasizing the nature of the lower gabbroic rocks as pure cumulates. While Figure 4b excludes rock influence by HTFZs, this is not the case for Figures 4c and 4d where the individual modal amounts of hornblende, orthopyroxene, and (magmatic) Fe-Ti oxides with crustal depth are shown. These plots clearly show that these typical late stage minerals do not play a significant role as primary minerals in the lower part of the gabbroic crust (LFG, Layered Gabbro Unit, MTZ), but rather as secondary phases formed by a magmatic process related to HTFZs under high water activities, as indicated by the high amount of magmatic hornblende (Figure 4c).

In the upper gabbros (UFG and DGT) the late stage phases become increasingly important as primary interstitial minerals (Figures 4b–4e), emphasizing the advanced differentiation of this part of the crust, which is in full

concordance with the plots of the mineral compositions with depth, as shown and discussed in Section 4.3. At the boundary between LFG and UFG the modal amount of the late stage minerals increases significantly, exactly (Figures 4c and 4e), where Mock, Ildefonse, et al. (2021) found the changing in the emplacement mechanisms, based on an interpretation of the microstructures. Figure 4f presents the grade of alteration which shows a typical hour glass structure, with stronger alteration in the lower and upper parts of the crust. As expected, rocks influenced by HTFZs show, in general, strong alteration effects.

3.3.1. Petrography of the Main Gabbroic Series

MTZ. While typical layered gabbros of this unit show features similar to those presented in the next paragraph, there are several gabbros with special features, with a trend to more coarser grained rocks and lack of foliation. In addition, this unit shows a stronger hydrothermal overprint compared to the overlying Layered Gabbro Unit (Figure 4). Beside gabbros, this unit contains, as usual for the MTZs in Oman, dunites, wehrlites, and troctolites (Figures 2g and 2h). The dunites are monomineralic, medium-grained rocks with equigranular, anhedral granular textures, composed exclusively of olivine (now 100% altered to serpentine) and traces of spinel. Since these rocks form coherent layers within layered series of the MTZ (Figures 2g and 2h), we assume that these rocks were formed by accumulation of olivine in primitive, parental melts, and not by mantle/MORB melt interaction. Very similar rocks have been recorded in the OmanDP program drill cores of crust/mantle sites (CM sites; Kelemen et al., 2020). A troctolite sampled within this unit is highly altered (80%), coarse grained, with a seriate, granular texture. This rock shows a foliation parallel to the general layering observed in this unit, and bears olivines with a characteristic skeletal structure (harrisitic). We discuss this in Section 4.1.

Layered Gabbro Unit. By far most of the rocks within this unit are medium-grained, monotonous olivine gabbros and olivine-bearing gabbros with granular texture consisting of olivine, plagioclase, and clinopyroxene formed during cotectic crystallization (Figure 5). Rare within this unit are gabbros without olivine and troctolites. Phases are mostly anhedral to subhedral, with plagioclase having aspect ratios rarely in excess of 2:1. Some olivines show a harrisitic structure, implying rapid crystal growth (Figure 6c). Grain boundaries are gently curved or straight, often showing 120° contact angles, indicating a moderate degree of textural re-equilibration and implying a relatively slow cooling. Foliations are parallel or sub-parallel to the layering, and plastic deformations have not been observed. A characteristic feature of these gabbros is that they in general do not show typical interstitial late stage parageneses with hornblende, Fe-Ti oxides, and orthopyroxene, which are so often observed in gabbros from slow-spreading ridges. Clinopyroxenes in olivine gabbros distinctly larger than the matrix crystals showing poikilitic structures, which are observed in deep gabbros from Hess Deep at EPR (Lissenberg et al., 2013) and interpreted there as evidence for pervasive melt/rock interaction, are not observed within the Layered Gabbro Unit. But another characteristic rock type well-known from the IODP 345 drilling expedition at Hess Deep was found in the Wadi Gideah transect: troctolites with clinopyroxene oikocrysts with special features. While the plagioclase chadacrysts within the oikocrysts lack any orientation, the troctolitic matrix is highly foliated, wrapping around the oikocrysts (Figures 6a and 6b). We discuss this in Section 4.1. In close proximity of HTFZs we observed in the layered gabbro the record of hydrous partial melting triggered by the percolation of hydrothermal fluids on grain boundaries. We focus on this in Section 3.3.2.

Foliated Gabbro Unit. This unit consists mostly of olivine gabbro with granular texture. Compared to the layered gabbros, the foliated gabbros show a significantly smaller grain size (Figures 4a and 5b), and the layering disappears. Further differences from the layered gabbros are the structure of plagioclase, which is generally more elongated than in the layered gabbros, with aspect ratios from 2:1 to 5:1, and the presence of interstitial late stage minerals like brown hornblende, orthopyroxene, and Fe-Ti oxides, as shown in the mode plot against crustal height (Figures 4c–4e) and in the microphotograph of Figure 5b. Like the layered gabbro, the foliated gabbro shows strong foliations but in combination with a lineation and with variable directions, with a general steepening with crustal height. It is noteworthy that there is no gradual change between these two types of gabbro. In the ∼100 m thick transition between both units, we observe both medium-grained layered gabbros with foliation sub-parallel to the Moho and fine-grained foliated gabbros with variable foliation/lineation. As in the layered gabbros, no plastic crystal deformation has been observed. A special difference in the petrographic features between the foliated gabbros from the LFG and the UFG has not been observed, except a sharp increase in the modal amount of interstitial late stage minerals as outlined in Section 3.3. and shown in Figure 4.

DGT—Gabbros. The most common gabbros of this unit are medium-grained hornblende-oxide gabbros with inequigranular, subhedral granular to poikilitic textures. Because they are characterized by the presence of irregular

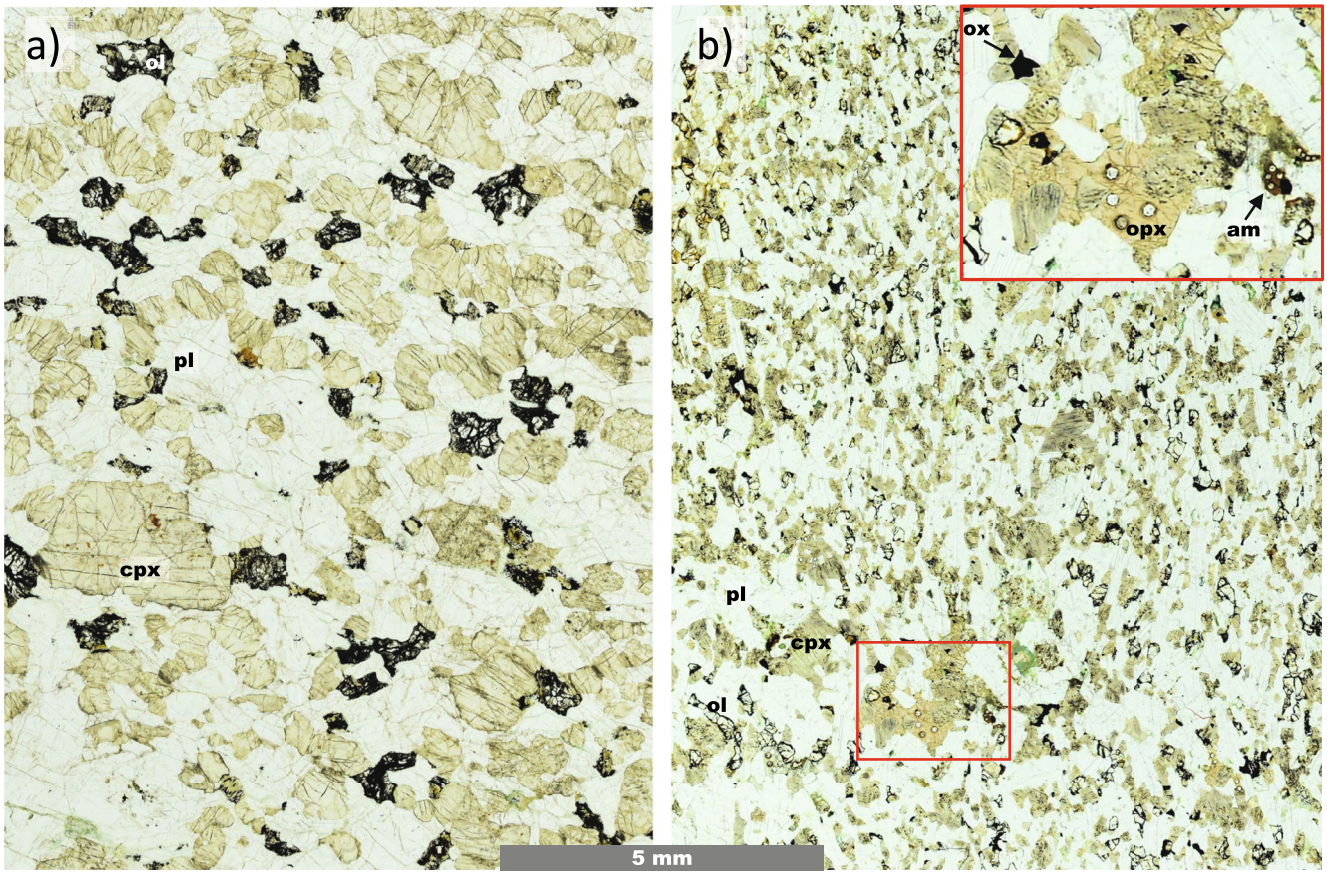

Figure 5. Microphotographs of typical layered (a) and foliated gabbro (b) at identical scale. Note the marked difference in grain size. The direction of foliation in (a) is sub-horizontal and in (b) sub-vertical. Minerals of the main stage (cotectic) crystallization are olivine (ol), plagioclase (pl), and clinopyroxene (cpx). Interstitial minerals only occur in the foliated gabbros, as demonstrated in (b). A zoom-in of a typical late-stage paragenesis marked by a red rectangle in the lower part of the picture shows the presence of orthopyroxene (opx), amphibole (am), and oxide (ox). Plane-polarized light. Samples: OM10-A26 (a) and OM10-A18 (b).

domains/patches with significant variations in grain size, texture, and mineral mode, they are named "varitextured gabbro" (see above). A typical feature of these gabbros is the presence of both poikilitic (subophitic) and granular textural domains within one thin section. Here, clinopyroxene forms mm-sized, poikilitic crystals containing plagioclase as chadacrysts. These poikilitic domains give the rocks a spotty appearance, which can be easily observed in the field (see Figure 3i in Müller et al., 2017). Granular domains evolved around these spots, consisting of plagioclase, hornblende (often with relics of clinopyroxene), and interstitial Fe-Ti oxide. Olivine is very rare. Under the microscope, these rocks can easily be distinguished from the underlying foliated gabbros, by (a) prismatic, often poikilitic hornblendes, (b) the presence of poikilitic and granular domains, and (c) lack of any preferred crystallographic orientation. Plagioclase occurs in two variants; as relatively small euhedral chadacrysts within the clinopyroxenes, and as much larger subhedral grains within the granular matrix showing a marked zoning (see Koepke & Zhang, 2021, for details). While the gabbros from the lower units are relatively fresh, the gabbros of the DGT are in general highly altered, with an average alteration intensity of 60% (for details see Table S1 in Supporting Information S1, PANGAEA data repository; Koepke, Garbe-Schönberg, et al., 2021). In some rocks, clinopyroxenes and/or plagioclase show a skeletal structure implying rapid growth (e.g., Holness, 2014). Microphotographs of typical varitextured gabbros from this area can be found in Figure 4 of Müller et al. (2017; from the Wadi Gideah) and in publications related to the GT3 core of the OmanDP (Figures 7 and 8 in France et al., 2021; Figures in Kelemen et al., 2020).

DGT—Basaltic Dikes. All basalts of the DGT show a granoblastic overprint, mostly in amphibolite facies but in some cases also in granulite facies (Figure 6e). They show a typical hornfelsic appearance with microcrystalline, granoblastic texture consisting of green and brown hornblendes (sometimes poikiloblastic), granular plagioclase, and granular Fe-Ti oxides. The former basaltic texture, which can be characterized as intersertal or intergranular,

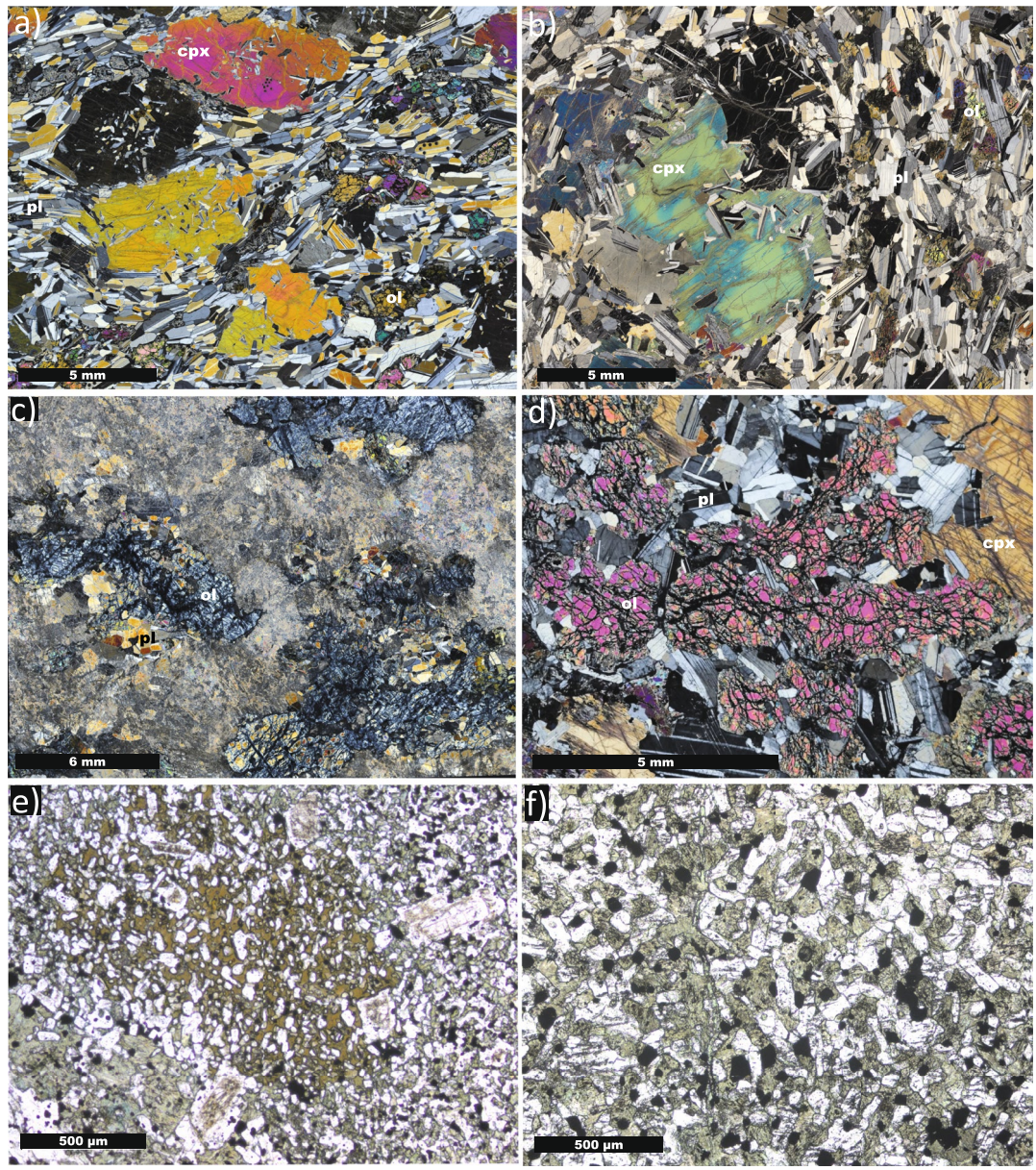

Figure 6. Microphotographs of special rock samples from the Wadi Gideah transect (left column) and from the East Pacific Rise (EPR) (right column), for comparison. For abbreviations, see Figure 4. (a) Troctolite with clinopyroxene oikocrysts from the Layered Gabbro Unit (H.a.M = 2,560 m). While the plagioclase chadacrysts lack any orientation, the troctolitic matrix is highly foliated, wrapping around the oikocrysts. Cross-polarized light. Sample: OM15-24. (b) Very similar features can be observed in layered gabbros drilled by International Ocean Discovery Project (IODP) at Hess Deep, EPR. Sample 345-U1415 J-5R-1, 117–120 cm. (c) Troctolite with cm-sized olivines showing skeletal structure (harristic). Most of the olivine and the plagioclase is altered. Cross-polarized light. Sample: OM15-13 (H.a.M = 61 m). (d) Very similar features can be observed in layered gabbros drilled by IODP at Hess Deep, EPR. Sample 345-U1415 J-11R-1, 22–24 cm. Cross-polarized light. (e) Former basalt from the dike/gabbro transition (DGT) (H.a.M = 4,627 m), now recrystallized under granulite facies with typical granoblastic texture consisting of poikiloblastic amphibole (brown and green colors), enclosing newly formed plagioclase (small, whitish) and Fe-Ti oxides (black). Enclosed larger plagioclases with brownish fillings are former phenocrysts, which survived as relics. Plane-polarized light. Sample: OM10-A12-2c. (f) Corresponding "granoblastic dike" from the DGT drilled at Site 1256 by IODP in 15 Ma old EPR crust, showing the same paragenesis. Plane-polarized light. Sample: 335-U1256D-Run12-RCJB-RockA.

is completely overprinted. Only some former phenocrysts survived as relics, occurring as euhedral grains with brownish fillings (Figure 6e). These "granoblastic dikes" are interpreted as former, hydrothermally altered basalts from the conducting boundary between the AML and the sheeted dike sequence within DGTs from fast-spreading mid-ocean ridges. Such rocks are well known from the EPR and from the Troodos and the Oman ophiolite (e.g., France et al., 2009; Gillis, 2008; Koepke et al., 2008; Zhang et al., 2014).

3.3.2. Petrography of the HTFZ Rocks

The petrographic record of the influence of HTFZs cutting the crustal units at many places is visible in two respects: (a) the rocks involved in forming the crustal units are in general highly to totally altered, mostly in greenschist facies, sometimes resulting in "metagabbros," consisting exclusively of greenschist facies minerals. Often, these rocks bear relics of magmatic minerals, sometimes developed as pseudomorphs (e.g., iddingsite in terms of olivine). The corresponding rocks are not further considered here (for more details see Table S1 in Supporting Information S1, PANGAEA data repository; Koepke, Garbe-Schönberg, et al., 2021). (b) The interaction of hydrothermal fluids with existing rocks at very high temperatures resulted in magmatic processes, which either formed completely new rocks or which modified host rocks by the development of crosscutting magmatic veins. For both cases we present details in the following.

As can be seen in Figure 4, which presents petrographic data with crustal height, the most common features related to magmatic processes with HTFZ influence are the presence of (magmatic) hornblende and an increase in grain size. Interestingly, all gabbros of the layered gabbro unit containing magmatic hornblende are related to an HTFZ process (Figure 4). This means that the whole ~2,500 m thick Layered Gabbro Unit is virtually free of magmatic hornblende in terms of primary magmatic accretion, which is in contrast to the Foliated Gabbro Unit, where primary hornblende occurs in late stage interstitial parageneses. Rocks related to HTFZ influence are, in contrast to the "normal" gabbros, significantly more altered. Most of the primary brown hornblende is converted to secondary green hornblende, but relics of brown hornblende can be observed in most of these samples.

Typical rocks are hornblende gabbros with prismatic brown hornblendes, tabular plagioclases, and coarse-grained to very-coarse-grained, granular textures, lacking any preferred crystallographic orientation. Special melanocratic rocks crosscutting layered gabbros can be found in the multiple HTFZs at H.a.M. from 1205 to 1237 m (Figure 3e). The hydrothermal alteration in these gabbros (OM12-Hy032A to D) is extremely intense (70%–85% for most rocks), and has converted most of the brown hornblendes to green hornblende. The brownish rock visible in Figure 3c (OM12-Hy55B) is coarse-grained, isotropic olivine gabbro with spectacular cm-sized olivines showing skeletal structure. The olivine is completely serpentinized, due to later hydrothermal overprint (alteration intensity of this rock: 85%). This gabbro can be characterized as "wehrlitic", since plagioclase shows a relatively small modal content (15%), representing interstitial fillings, while olivine and prismatic clinopyroxene form the main granular network. Since none of these rocks characterized above are found as coherent layers within the layered gabbro, these rocks are of special significance.

From the magmatic veins crosscutting layered gabbros found within HTFZs we describe two of them in detail in the following, exposed in the multiple HTFZ at H.a.M from 1205 to 1237 m. The first one visible in sample OM12-027 is shown in Figure 7. The contact between host rock, which is a typical layered olivine gabbro, and the magmatic vein is homogeneous and gently sutured, implying that the host gabbro was more a mush than a solid rock when the magmatic vein intruded. The vein rock is a hornblende diorite lacking any foliation, which is quite evolved, expressed by poikilitic orthopyroxene and brown hornblende with inclusions of apatite, as well as granular oxides. Of special significance is the presence of characteristic microstructures within the host gabbro adjacent to the magmatic vein, which provides evidence that hydrous partial melting occurred. This is confirmed by an electron backscattered image in Figure 7, showing characteristic An-enriched zones at the grain boundaries between plagioclases in the host gabbro near the contact. Such zones, in combination with tiny interstitial formations of amphibole, are the product of a partial melting reaction, triggered by hydrous fluids on grain boundaries. These features are reported from many gabbros from recent oceans (Koepke et al., 2004, 2005) and from the Oman ophiolite (Koepke et al., 2014). EPMA profiles through such zones show the characteristic asymmetric An-enrichment of such zones, as well as the depletion of K_2O and TiO_2 (Figures 7c and 7d), which is a consequence of the interaction with hydrothermal fluids impoverished in these elements. This archetype of partial melting reaction in gabbros triggered by hydrous fluids is also verified experimentally, showing, beside the characteristic concentration profiles in the zones of the enriched plagioclase, also the dislocated nature of this melting reaction. New plagioclase crystallizes on grain boundaries between host plagioclases, and new mafic

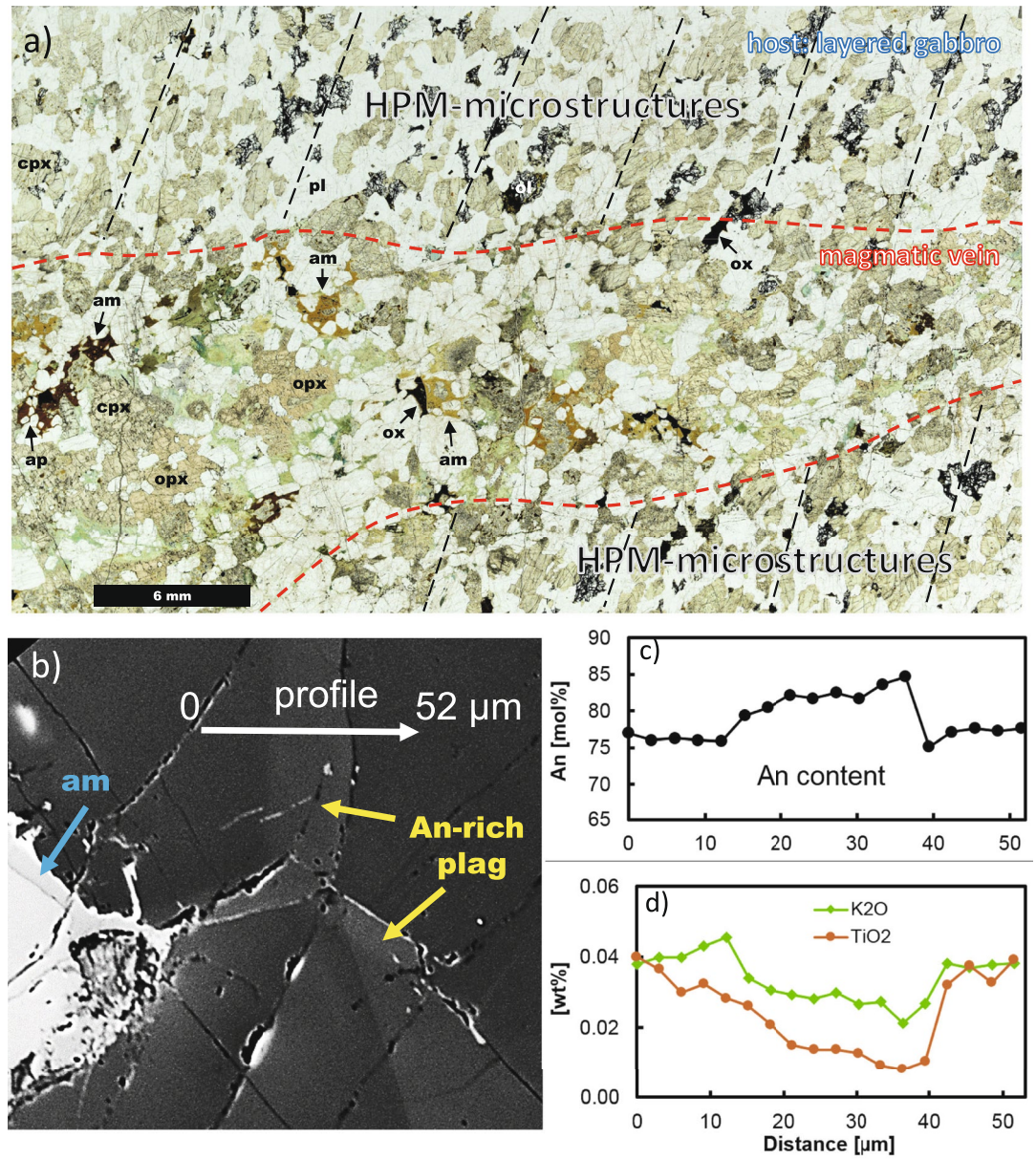

Figure 7. (a) Whole thin section scan of a layered olivine gabbro hosting a cm-thick magmatic vein consisting of hornblende diorite within the HTFZ at H.a.M. from 1205 to 1237 m. The layering is indicated by dashed lines. Contacts between host rock and vein are homogeneous and sutured, implying that the host gabbro was more a mush than a solid rock. The hornblende diorite is quite evolved, bearing poikilitic orthopyroxene and brown amphibole as well as granular oxides. The evolved nature is also demonstrated by the presence of apatite (ap), occurring as inclusions within the brown amphibole. The host gabbro adjacent to the magmatic veins shows characteristic microstructures evidencing that hydrous partial melting proceeded, as demonstrated in (b). (b) shows an electron backscattered image of grain boundaries between plagioclases in the host gabbro near the contact, where zones of An enrichment were formed. Such zones show a characteristic compositional evolution as demonstrated in the EPMA profiles across such a zone for An content and for K_2O and TiO_2, shown in (c) and (d), respectively. See text for details. Sample OM12-27. For abbreviations of the minerals see Figure 4.

phases crystallize at the contact to host mafic phases (Wolff et al., 2013). We discuss the consequences of this reaction in Section 4.6.

Another magmatic vein from the same HTFZ crosscutting layered olivine gabbro is shown in Figure 8 (sample OM12-Hy80.5). The vein rock is a medium-grained, isotropic hornblende diorite with an isotropic, granular tex-

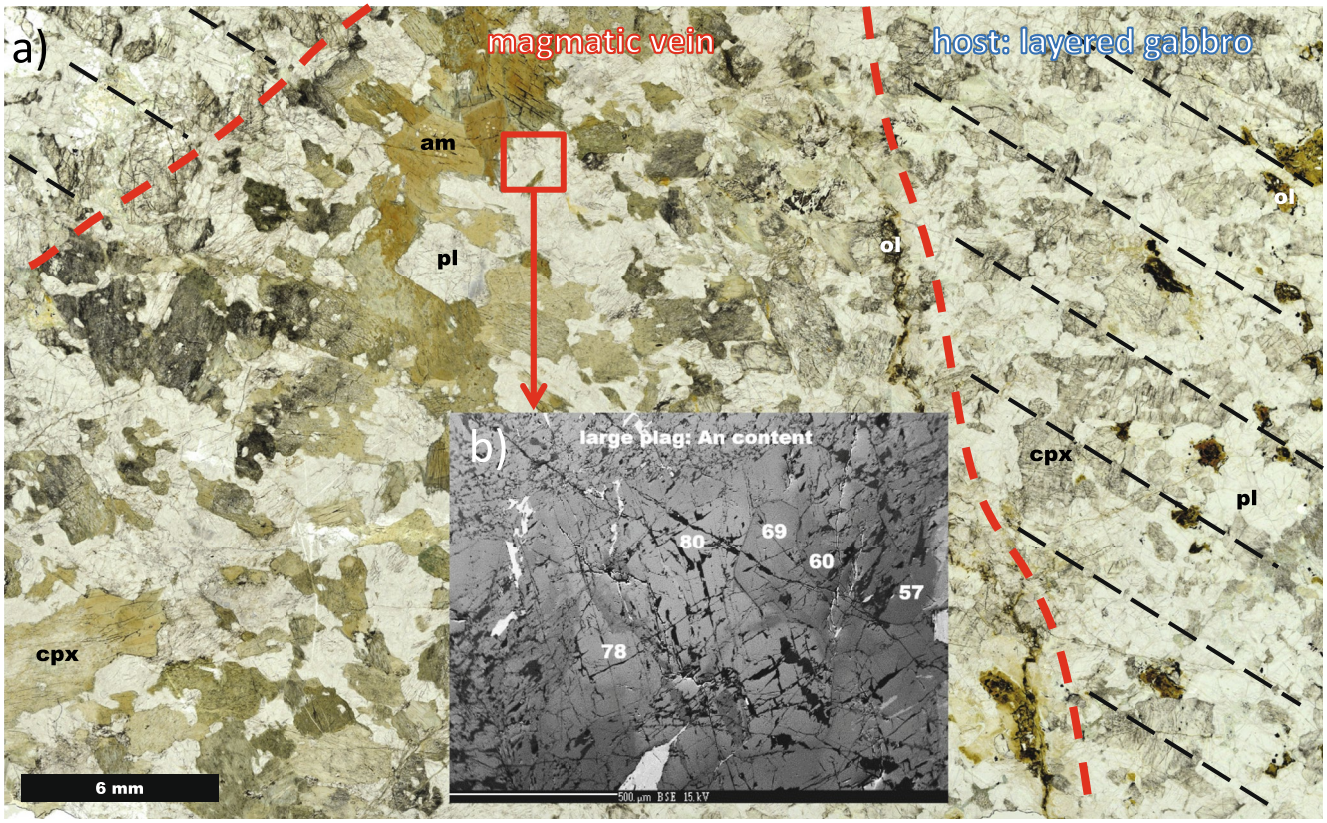

Figure 8. (a) Whole thin section scan of a layered olivine gabbro hosting a cm-thick hornblende diorite vein within the HTFZ at H.a.M. from 1205 to 1237 m. The layering is indicated by dashed lines. The hornblende diorite bears plagioclase with cores showing the same composition as the plagioclase in the host gabbro, while the rims are lower in An, as shown in the electron backscattered image in (b). The numbers in (b) refer to the An content in one large plagioclase (plag) grain. This, and the presence of primary clinopyroxene relics within the magmatic amphiboles in the vein, imply that the hornblende diorite emplacement was not a simple vein filling by a distal melt/magma, but the result of a reactive replacement process. See text for details. Sample OM12-Hy80.5. For abbreviations of the minerals see Figure 4.

ture. As shown in the EBSD image in Figure 8, the hornblende diorite bears plagioclase with cores showing the same composition as the plagioclase in the host gabbro, while the rims are lower in An. This, and the presence of primary clinopyroxene relics within the magmatic hornblendes in the vein, imply that the hornblende diorite emplacement was not a simple filling of a crack in the solid gabbro by a distal melt/magma, but the result of a reactive replacement process.

3.4. Mineral Analysis

The high number of analyzed samples (140 analyzed thin sections; 604 mineral averages; >9,300 single analyses) enable a statistically meaningful evaluation of the evolution of the main stage crystallization within the Oman paleocrust. Details are presented in Table S2 in in Supporting Information S1 (PANGAEA data repository; Koepke, Garbe-Schönberg, et al., 2021). Plots for olivine, plagioclase, and clinopyroxene with crustal height are shown in Figure 9. Only core analyses are presented, representing the evolution of the main stage crystallization. Figure 9 also includes samples influenced by HTFZs (see Section 3.3.2). The main criterion for this assignment was that brown hornblende of magmatic origin existed within samples from HTFZs. It should be noted that for several crustal heights more than one sample exists (i.e., nine samples for 5,009 m H.a.M.), resulting, in part, in a considerable scattering of the data. The recorded mineral evolutionary trends with crustal height are rather similar, both for major elements (Mg# in olivine and clinopyroxene; An content in plagioclase) and minor elements (NiO in olivine; TiO_2, Cr_2O_3, Na_2O in clinopyroxene; Figure 9).

Variations in the merely ~160 m thick MTZ are strong, showing both a very depleted and a rather evolved character: for example, the Mg# for clinopyroxene varies from 88.8 (the highest value for the whole profile) down to 77.8 and the An content in plagioclase varies from 87.7 mol% (the highest value in the profile) down

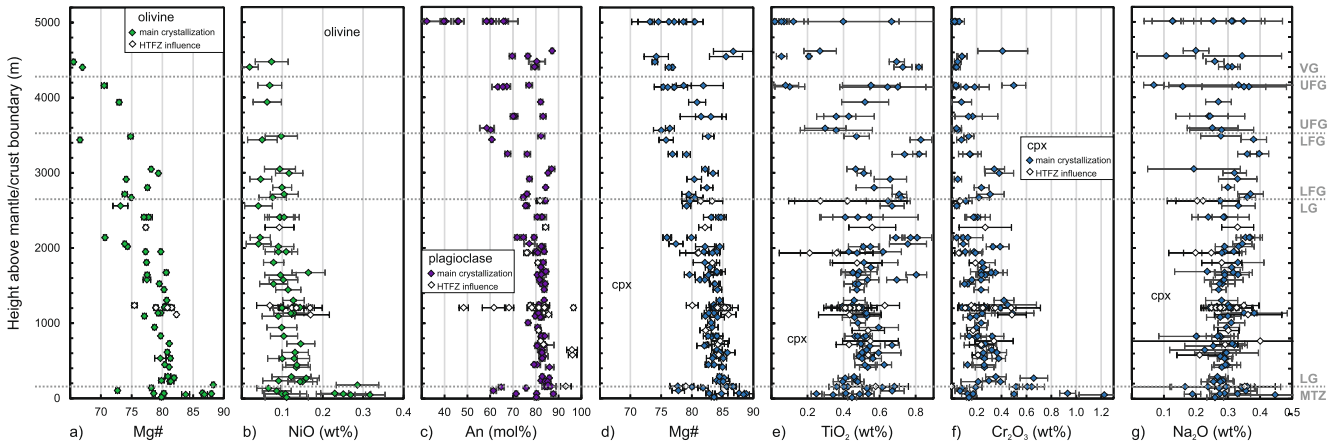

Figure 9. Geochemical depth logs for average mineral major element content: olivine (a and b), plagioclase (c), and clinopyroxene (d–g). Only core analyses are plotted. Most data points represent the evolution of the main stage crystallization (filled symbols), but samples influenced by hydrothermal fault zones are also shown (open symbols). For the H.a.M. 5,009 m, more plagioclase analyses exist, with values below 30 mol% (16.5 mol% is lowest An content). These analyses are not shown in Figure 9c in order to display better the part with higher An contents, which is more relevant for the crustal evolution. Errors correspond to one standard deviation. The boundaries between the crustal units are shown.

to 61.5 mol%. The depleted character of the minerals from the MTZ is also expressed by the highest values for Cr_2O_3 in clinopyroxene and NiO in olivine (Figure 9). Rocks from the MTZ analyzed are wehrlite, troctolite, olivine gabbro and gabbro.

The mineral trends in the 2.5 km thick Layered Gabbro Unit are straight and relatively steep, lacking significant variations (Figure 9). Mg# in olivine and clinopyroxene vary from 70.7 to 88.3 and 75.9 to 85.8, respectively, and An in plagioclase varies from 71.8 to 86.9 mol%. A large scattering in An content can be observed with respect to those hornblende-bearing samples of the Layered Gabbro Unit influenced by HTFZs; here, plagioclase varies significantly with both very low and very high An contents (48.4–96.6 mol%). Rocks from the Layered Gabbro Unit analyzed are troctolite, olivine gabbro, gabbro, oxide gabbro and metagabbro with respect to magmatic relics.

When examining the foliated gabbro further up in the profile, two features of the mineral evolutionary trends change. First, the slope of the trends flattens, and second, the data show a much wider scattering (Figure 9). Mg# in olivine and clinopyroxene varies from 66.6 to 79.4 and 75.0 to 83.4, respectively, and An in plagioclase varies from 58.6 to 87.0 mol%. For the LFG we observe a continuation of the trends from the Layered Gabbro Unit, which are best expressed in the evolutionary trends for clinopyroxene (Figure 9). For the UFG, however, the general evolutionary trend ceases, changing to a complex data scattering where no clear trend is obvious. An exception is the compositional evolution of olivine, which seems to follow the trend from beneath. But there are only two data points at this crustal level, since the presence of analyzable olivine in the gabbros from a high crustal level is rare; this is also due to the much stronger alteration in this horizon, compared to the lower part of the plutonic crust (Figure 4f). Rocks from the Foliated Gabbro Unit analyzed are olivine gabbro, gabbro, and oxide gabbro.

Finally, in the DGT, where the foliated gabbros change to varitextured, the mineral evolutionary trends are much more diffuse with extreme scattering in the data, varying from very primitive to highly differentiated compositions (Figure 9). This is especially expressed by the An content in plagioclase which varies from 16.5 to 87.2 mol%. It is noteworthy that the An content in plagioclase from the varitextured gabbro OM10-A13 (87.2 mol%) is the second highest in the whole profile (rocks influenced by HTFZs excluded), only exceeded by a plagioclase in a troctolite from the MTZ (87.7 mol%). A similar situation is reflected by the Mg# in clinopyroxene: clinopyroxene cores in varitextured gabbro OM10-A13 show an Mg# of 86.7. Slightly higher values are only recorded from the MTZ from clinopyroxene cores in an olivine gabbro, wehrlite, and troctolite. We will focus on this in Section 4.3. in the discussion. Rocks from the DGT analyzed are olivine gabbro, gabbro (mostly typical varitextured gabbro), oxide gabbro, quartz diorite, tonalite and trondhjemite. Minerals from highly evolved rocks like tonalites and trondhjemites are not included in Figure 9.

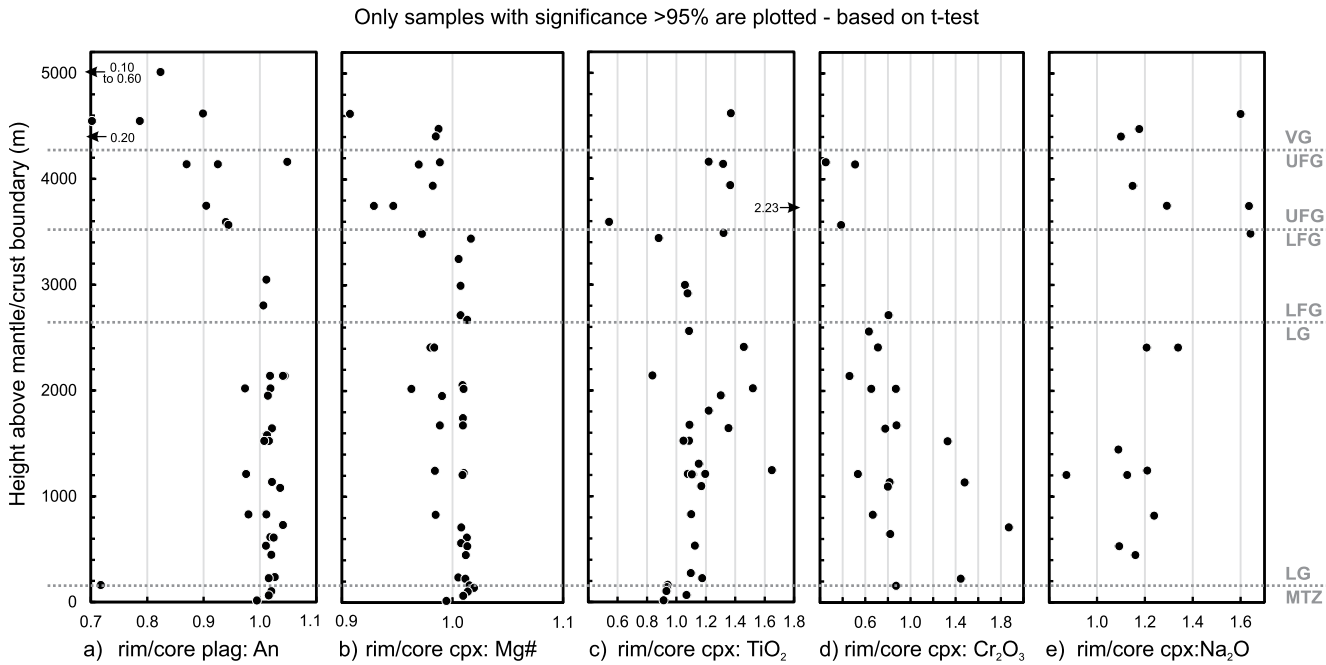

Figure 10. Factors rim analysis divided by core analysis plots against crustal height for plagioclase An content (a), clinopyroxene Mg#, TiO_2, Cr_2O_3, and Na_2O (b–e). All analyses are averages. Only rim/core pairs shown passed the *t*-test and are regarded as statistically meaningful (95% significance level). The boundaries between the crustal unit are shown. For details see text.

In Figure 9, we also included those samples where an influence of HTFZ was identified by the presence of magmatic hornblende (large granular, often poikilitic grains; main constituent of magmatic veins cutting the layered gabbro as shown in Figures 7 and 8). The depth logs for olivine and clinopyroxene compositions are without significant anomalies, except for a large scattering in the TiO_2 concentrations for some clinopyroxene (Figure 9e). Plagioclase, however, shows in these rocks a broad compositional variation to very low and to extremely high An contents, which is especially shown for the large HTFZ at a crustal height of 1205 m H.a.M., where variations from An 96.6 to 48.4 mol % occur (Figure 9c).

Mineral zoning is shown in Figure 10, where rim analysis divided by core analysis is plotted with crustal height. As reported in Section 2.4, the only rim/core pairs considered are those which passed the *t*-test and are regarded as statistically meaningful (95% significance level). Olivine is virtually unzoned with respect to Mg# except for one rim/core pair of slightly normal zoning in the foliated gabbros. With respect to An content, plagioclase shows a marked inverse zoning in the MTZ and Layered Gabbro Unit (median rim/core value is 1.016), changing to unzoned conditions in the LFG, finally transitioning to normal zoning in the UFG and DGT (Figure 10a). Concerning the Mg# in clinopyroxene, most core/rim factors, by far, reveal a slight inverse zoning trend in the lower part of the gabbroic crust (MTZ, Layered Gabbro Unit, LFG; median rim/core value is 1.009), switching quantitatively into normal zoning when entering upsection the UFG and DGT (Figure 10b). In contrast, TiO_2 in clinopyroxene shows, in general, a slight normal zoning behavior in the lower part of the Layered Gabbro Unit up to ~1600 m H.a.M (core/rim median is ~1.09). Above this height, the grade of normal zoning increases significantly with a core/rim median of 1.22 (maximum value is 2.23).

4. Discussion

4.1. Comparison With Lower Crustal Rocks From Hess Deep (EPR)

In Figure 6 we present petrographic features of rocks from all crustal levels of the Gideah transect, which are quite similar when comparing with corresponding rocks from the EPR. In Figure 6a we present olivine gabbros from the Oman Layered Gabbro Unit and from the Hess Deep (EPR) lower crust drilled by IODP Expedition 345 (Gillis, Snow, Klaus, & the Expedition Scientists 345, 2014), showing a special phenomenon: both rocks contain clinopyroxene oikocrysts bearing plagioclase chadacrysts that lack any orientation, swimming in a troctolitic

matrix which is highly foliated and wraps around the oikocrysts. An obvious formation scenario would be that in a plagioclase/melt mush, heterogeneous crystallisation produces clinopyroxene oikocrysts enclosing plagioclase crystals, which are after melt extraction/compaction wrapped by a planar matrix. Such a crystallization scenario proceeds under isothermal conditions, or with slightly dropping temperatures.

However, the matrix in these rocks both from Oman and Hess Deep, is troctolitic, indicating that the crystallization temperature was higher, since from experimental phase equilibria in primitive MORB systems it is well-known that olivine and plagioclase crystallizes before clinopyroxene (at least at low to moderate water activities). So, a simple cooling/compaction model cannot work for the formation of these special rocks. We suggest a two-stage process for the formation of these oikocryst-bearing troctolites. First, at relatively lower temperatures under cotectic crystallization conditions, clinopyroxene crystallizes in a static regime enclosing smaller plagioclase crystal, showing random orientation in the clinopyroxenes. In a second stage, these clinopyroxene oikocrysts accumulate and are transported into a troctolitic crystal mush existing at relatively higher temperature (clinopyroxene not on the liquidus), where melt extraction/compaction leads to the planar fabric. Such a two-stage scenario is in accord with the model of layer formation of typical layered gabbro from the Oman deep crust of Mock et al. (2020). This model suggest in a first step crystallization at the margin of individual melt reservoirs in the deep crust. In a second step, the crystallized material at the wall of the melt reservoir wall becomes unstable and is transported by density currents to the bottom of the melt reservoir, which may experience occasional magma replenishment. This explains the prevailing higher temperature with the potential of forming troctolitic mushes (for details see Figure 13 in Mock et al., 2020). Compaction after melt extraction would lead to the planar fabric of the troctolitic matrix, which is observed in the corresponding rock. That these special petrographic records are observed both in Oman and at Hess Deep underlines the similarities in magmatic accretion processes of both ridges.

A good accordance can also be observed in terms of the presence of skeletal and dendritic ("harrisitic") olivines found both in layered troctolites from the Oman MTZ, and in deep layered sequences drilled at Hess Deep (Gillis, Snow, Klaus, & the Expedition 345 Scientists, 2014) as demonstrated in Figures 6c and 6d. Experimental studies suggest that such olivines were formed by in-situ crystallization and grew relatively rapidly under conditions of strong supersaturation or magmatic undercooling (e.g., Lofgren & Donaldson, 1975). It is obvious that the presence of such delicate structures strongly suggests in-situ crystallization and is not in accord with a ∼5 km long, highly deformative transport of crystal mushes, which once formed in the AML. A similar conclusion is valid for the formation of the oikocryst gabbros in troctolitic matrix mentioned above. It is highly improbable that such filigree structures survived a km-long mush suspension under deformative conditions.

Another similarity between the Wadi Gideah gabbros and those of Hess Deep is related to orthopyroxene-forming reactions in gabbros in the lowermost part of the crust. In primitive gabbros from the lower crust of Hess Deep orthopyroxene occurs quite often as prismatic crystal (e.g., Coogan, Gillis, et al., 2002; Gillis, Snow, Klaus, & the Expedition 345 Scientists, 2014), which is not in accord with the fact that primitive MORBs are not saturated with orthopyroxene. Therefore, Coogan, Gillis, et al. (2002) suggested that these orthopyroxenes are a product of interaction between primitive MORB melts and shallow mantle rocks. In gabbros from the MTZ of the Wadi Gideah profile, we observed petrographic features, implying that similar reactions occurred. In olivine gabbro OM10-A32 prismatic orthopyroxene is mantled by clinopyroxene, and in olivine gabbro OM15-40 which is associated with cpx-bearing dunite, one prismatic orthopyroxene grain was formed directly at the boundary between both lithologies. Both examples imply that prismatic orthopyroxenes in these rocks are formed by reactions with mantle instead of simple crystallization in a primitive MORB, emphasizing close similarities in magmatic process at the base of the crust of Oman and of EPR. However, the frequency of these rocks is different: while such rocks are very common in the layered gabbros recovered from Hess Deep (Gillis, Snow, Klaus, & the Expedition 345 Scientists, 2014), such rocks occur in the Wadi Gideah profile only within the MTZ and are absent in rocks from the Layered Gabbro Unit.

A further example of good lithological accordance between the Oman paleocrust and the EPR is the presence of granulite facies, granoblastic hornfelses in the DGT (Figures 6e and 6f), underlining close similarities with respect to the geodynamics of AMLs (i.e., vertical fluctuations and their consequences with respect to anatectic processes and MORB contamination, for details see Koepke & Zhang, 2021).

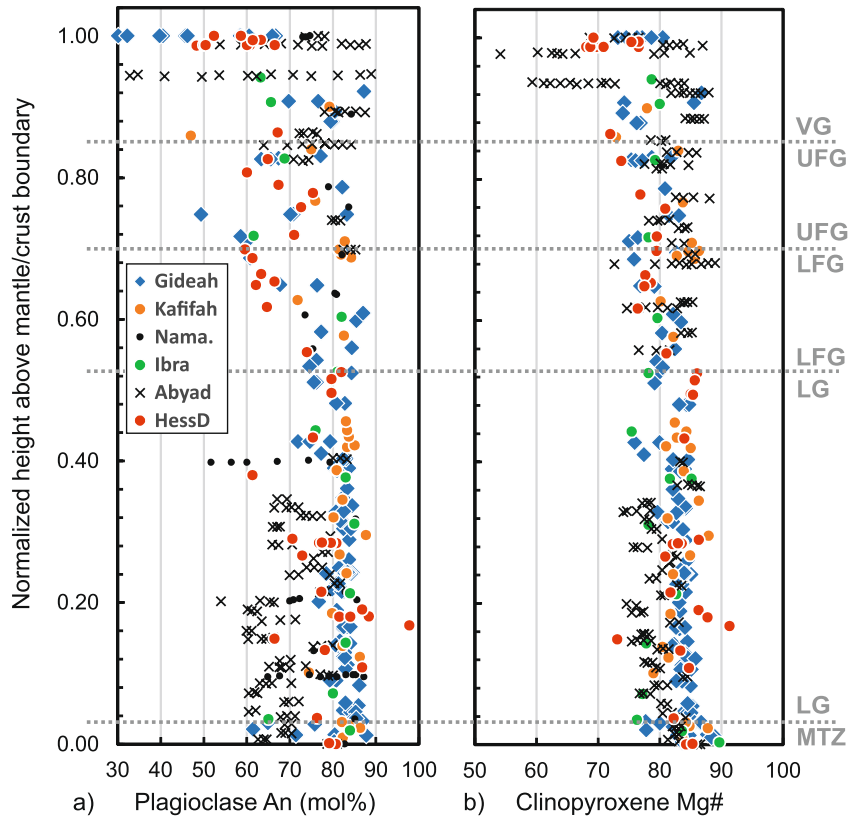

Figure 11. Geochemical depth logs for An content in plagioclase and Mg# in clinopyroxene from various sites in the Oman Ophiolite (Wadis Gideah, Kafifah, Namarah, Abyad, and Ibra area), and from Hess Deep at East Pacific Rise (EPR). The boundaries between crustal units shown are for the Wadi Gideah as estimated in this study. Data sources: Wadi Gideah–this study (averages from core analyses; compositions related to HFFZs are not considered); Wadi Kafifah—VanTongeren et al. (2021); Wadi Namarah—Coogan (2014); Wadi Abyad—MacLeod and Yaouancq (2000), Browning (1982); Ibra area—Pallister and Hopson (1981); Hess Deep—Lissenberg et al. (2013).

To summarize, we observed very similar features with respect to rock-forming processes between the Wadi Gideah profile and the EPR, emphasizing the close similarity in terms of magmatic accretion between the Oman paleoridge and the actual EPR. Together with the five points listed in Section 1.4, it is obvious that the Oman paleocrust shares many more similarities with the modern EPR than with a spreading ridge in a typical region of subduction zone initiation, that is, the Izu-Bonin-Mariana crust, which is often used as a modern analogue for the Oman paleocrust (e.g., Ishizuka et al., 2014). A requirement for this assessment, however, is the exclusion of those processes related to the magmatic Phase 2 of the Oman paleo ridge accretion, which include the formation of boninites, gabbronorites, and large felsic intrusions, those characteristic lithologies which are absent in the Wadi Gideah.

4.2. Comparison With Other Crustal Profiles in the Oman Ophiolite and From the EPR

The comparison of the Wadi Gideah mineral trends with those of other crustal profiles available for the southern Oman ophiolite is shown in Figure 11. For comparison, the crustal height of all profiles has been normalized to 1.

The data set of the Wadi Abyad in the Nakhl-Rustaq block (Browning, 1982; MacLeod & Yaouancq, 2000) contrasts with the observations from this study, since in general the Wadi Abyad layered and foliated gabbros do not show a general trend of chemical evolution up section (Figure 11). Due to a sampling gap of about 400 m (correspond to a normalized crustal height from 0.43 to 0.56 in Figure 11), the overall trend can be divided into a lower and an upper trend. The trend for the lower 1 km (from 0 to 0.43 in Figure 11) of the crust shows a slight evolution to differentiated compositions, at least for the Mg#s of clinopyroxene and olivine, similar to the Wadi Gideah trend. The upper trend shows an evolution to more primitive compositions, especially for clinopyroxene,

which strongly contrasts with the observation in the Wadi Gideah. The uppermost hundred meters (from 0.93 to 1 in Figure 11) of the profiles correspond to the varitextured gabbros from the AML horizon with highly differentiated compositions, very similar to the observations in the Wadi Gideah. It should be noted that the Wadi Abyad plutonic crust is folded and has, in contrast to other Oman crustal sections, a reduced thickness of only ~2.5 km, implying that this section is not representative of the Oman paleocrust (see Section 1.3).

Profiles for An content in plagioclase for the Kafifah and Namarah wadis, which both run parallel to the Wadi Gideah in a distance of ca. 10 km to the west and east, respectively, are published in VanTongeren et al. (2021) and Coogan (2014). Both contrast with the Wadi Gideah profile, because they do not show an upward evolutionary trend (Figure 11). For the Wadi Kafifah profile two data points from the uppermost gabbros show more evolved compositions, similar to those plagioclases from the varitextured gabbros of the Wadi Gideah. Due to the lack of any petrographic specification, the missing data of other mineral parameters, and the relatively low sample resolution with crustal height, it is difficult to compare these profiles with those of the Wadi Gideah.

Pallister and Hopson (1981) published combined mineral data for different wadis from the Ibra area of the Wadi Tayin massif, which includes also data from the Wadi Gideah (for details see Section 1.3). Although their data set is very limited (only 16 samples) their profile fits quite well with the profile for the Wadi Gideah, with a very steep, near vertical trend in the layered gabbro and a distinct change to more evolved compositions for the upper gabbros.

From modern fast-spreading ocean crust a complete profile is available only from Hess Deep (Lissenberg et al., 2013) based on sampling by ROV in strongly faulted areas, which makes the assignments of samples to the exact stratigraphic height very difficult. The deeper gabbros show a strong scattering in their data with a general trend very similar to the Wadi Gideah profile, when ignoring outliers. With respect to An in plagioclase the Hess Deep trend is slightly shifted towards lower values, which is in accord with higher water activities in the parental melts of the Wadi Gideah gabbros (Koepke, Feig, et al., 2021; MacLeod et al., 2013; Müller et al., 2017), which shift the An content to higher values. For the upper gabbros, starting from a crustal height which corresponds to the transition between layered and foliated gabbros for the Wadi Gideah profile, both trends are quite similar (Figure 11), implying that advanced differentiation starts at both locations at the transition between lower and upper gabbros.

4.3. Differentiation Trends for the Wadi Gideah Transect–Upward, Downward, or Both?

Since magmatic differentiation is that process regarded as responsible for the observed lithological diversity and compositional variation in the lower oceanic crust, we aim in this section to explain the observed mineral trends with crustal depth shown in Figure 9 by fractional crystallization. For this we used the program COMAGMAT (Ariskin & Barmina, 2004), which accounts for the effects of water activity on olivine, plagioclase, and clinopyroxene, and is optimized for crystallization processes at shallow pressures. In order to reproduce the Wadi Gideah mineral trends of chemical evolution, we varied the initial melt composition as well as the H_2O content of the melt. As starting composition we used an experimentally derived MORB parental melt composition (example 2 of Kinzler & Grove, 1993). The same composition was used in MacLeod et al. (2013), for modeling the evolution of V1 basalts in the Oman ophiolite by fractional crystallization, and in Müller et al. (2017) for modeling the evolution of the varitextured gabbro in the frozen melt lens horizon located in the Wadi Gideah. MacLeod et al. (2013) corrected the Ti content of the experimental composition from 0.87 to 0.70, in order to match better typical primary MORB melts from subduction zone initiation settings, and we followed MacLeod et al. (2013) here. When using this composition in our COMAGMAT petrological calculations, the Mg# of first olivine or clinopyroxene have been too high in comparison to that of the lowermost gabbros from our profile, implying that the melts feeding the Wadi Gideah paleocrust experienced a pre-differentiation, either within the mantle or at the bottom of the crust, below or within the MTZ. For the latter option speaks the findings of the crust/mantle drillings within the ICDP OmanDP, where a 90 m thick pile of pure dunite was recovered at the base of the crust (Kelemen et al., 2020). This horizon could be interpreted as accumulated olivine, with the potential to decrease the Mg# of the parental melt feeding the crust, accordingly. In order to match the Mg#s calculated by COMAGMAT with those of olivine and clinopyroxene of the natural rocks from our profile, we changed the Mg# of the original starting composition of Kinzler and Grove (1993) from 72 to 66.

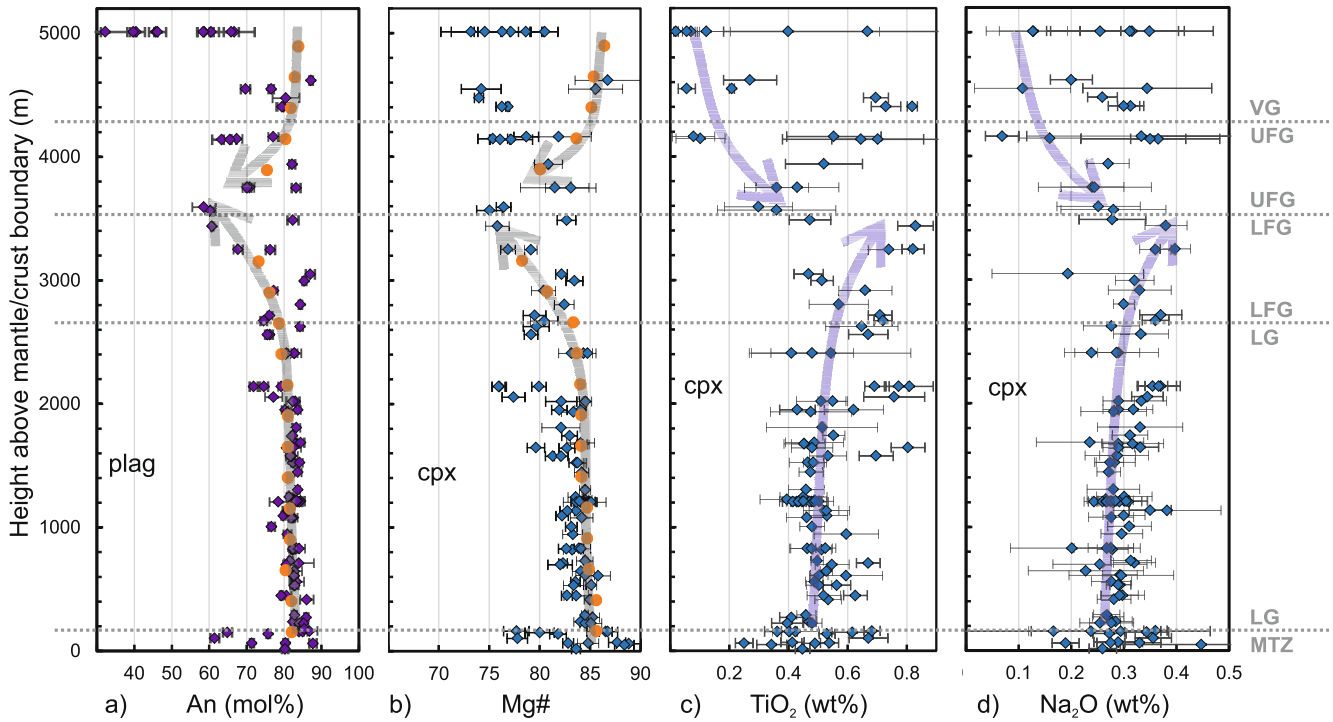

Figure 12. Geochemical depth logs for An in plagioclase (a), and for Mg#, TiO_2, and Na_2O in clinopyroxene (b–d). Differentiation paths evaluated via COMAGMAT (in gray) and individual COMAGMAT results (orange circles) are included for (a) and (b). COMAGMAT is not able to constrain the contents of minor elements in clinopyroxene, such as TiO_2 and Na_2O as shown in (c) and (d). The paths shown in (c) and (d) are simply the mirrored differentiation paths of (a) and (b), copied into the corresponding plots (c) and (d) (in blue). For fine adjustments of the paths, we widened the paths a little bit in the *x* direction, but did not change the direction of the paths. For details of the calculation procedure see text. The mineral data are those from Figure 9, with analyses related to HTFZs excluded.

We set 200 MPa for crystallization in the lower crust and 100 MPa for the mid crust, in order to correspond to the varying lithostatic pressure in the oceanic crust, and an initial oxygen fugacity corresponding to the quartz-fayalite-magnetite (QFM) buffer. We found that varying both pressure and oxygen fugacity had little effect. We set 0.8 wt% to be the initial amount of H_2O in the melt, which is in the range of the calculated water contents for Oman parental melts both from MacLeod et al. (2013) for the basaltic suite and from Müller et al. (2017) for varitextured gabbros. For our differentiation scenario by fractional crystallization we used an approach following the conclusions Mock, Ildefonse, et al., 2021, who suggested in-situ crystallization in the lower part of the plutonic crust (layered gabbro and LFG), and a vertical transport of melt or mush according to a glacier process in the upper part. Accordingly, for the COMAGMAT calculations we divided the whole gabbroic crust in two parts with different modes of fractionation/mixing: For the lower part, we simulated, in accord with the sheeted sill model, upward differentiation, starting at the mantle/crust boundary, and for the upper part we simulated downward differentiation starting in the AML horizon, in accord with the gabbro glacier model. Each differentiation step in our COMAGMAT calculation covers a crustal interval of 250 m. This value is entirely arbitrary, and does not correspond to any height of melt reservoirs or melt sills observed in the ocean crust, which are regarded to be much thinner (e.g., Carbotte et al., 2021; Detrick et al., 1987). For each step, our aim was to match the mineral compositions of plagioclase (An content) and clinopyroxene (Mg#) of the rock samples at the given crustal height. The calculated differentiation trends are presented in Figure 12. More explanations about the modeling procedure, including a table presenting all parameters/compositions of each fractionation and/or mixing step are presented in Supporting Information S1.

For the Layered Gabbro Unit, the mineral evolutionary trends are straight and very homogenous. Although very steep and nearly vertical, an evolutionary trend to more differentiated compositions with crustal height is clearly visible for all compositional plots (Figure 9). This can be best modeled by an upward differentiation, as is expected from the sheeted sill model for crustal accretion. The chosen conditions for the COMAGMAT modeling resulted in An contents and Mg# for clinopyroxene matching well the mineral compositions of the lowermost gabbros within the Layered Gabbro Unit. In order to reproduce the very steep trends, we simulated replenishments using

the following procedure: after the onset of cotectic crystallization, we mixed 50% of the residual post-crystallization liquid with 50% of liquid with the starting composition for each fractionation step. We used 10 steps for this procedure to match the mineral compositions at the uppermost level of the Layered Gabbro Unit. Since after each step the residual liquid is slightly more differentiated compared to the liquid from the previous step, we successfully reproduced the very steep mineral evolution trend of the natural gabbros. With this procedure, we simulated the process of accumulation of fractionated minerals within individual sills, where the slightly differentiated residual liquids move upwards, in accord with the observed general trend for upward differentiation.

The mineral trends for the Layered Gabbro Unit are not simple straight lines, but show some fluctuations, which can be, in part, interpreted as sites where the differentiation was more pronounced. This is best documented in the TiO_2 content of clinopyroxene (e.g., at 711, 1645, and 2,139 m H.a.M). For 2,139 m H.a.M., all parameters in Figure 9 (except Al_2O_3 in clinopyroxene) show a prominent inflection point to more evolved compositions, which we interpret as a horizon with advanced differentiation. Here, we sampled the only oxide-bearing gabbro in the whole Layered Gabbro Unit which are not influenced by an HTFZ. On the other hand, fluctuations pointing to more primitive compositions, which are best monitored in Cr_2O_3 in clinopyroxene and NiO in olivine, could be regarded as sites where the replenishment with fresh, primitive melt dominates. Such a horizon is at 1674 m H.a.M, where both olivine and clinopyroxene record slightly more primitive compositions compared to the average trend.

In Section 3.3, we showed that with the onset of the Foliated Gabbro Unit the amount of interstitially crystallized late stage minerals significantly increases, which we interpret in our model of upward differentiation as the onset of a stronger differentiation by fractional crystallization and a decrease in replenishment with fresh, primitive melt. Consequently, in our petrological modeling we halted the replenishment steps and a focused on advanced differentiation. As starting composition for this we used the residual melt from the last step of fractionation within the Layered Gabbro Unit. The result is a marked bending of the differentiation path to more differentiated compositions (Figure 12), which matches the natural trend.

We halted the simulation of upward differentiation at the boundary between LFG and UFG, since in the UFG obvious trends are not observable or are significantly blurred. This is exactly the boundary where the EBSD data for a subset of samples used in this study reveals a significant change in the magma emplacement mechanism, as reported in Mock, Ildefonse, et al. (2021). Their data suggest a hybrid accretion model with different mechanisms for the upper (UFG and DGT) and lower plutonic crust (LFG and Layered Gabbro Unit). For the lower part, these authors suggest *in situ* crystallizing of individual magma reservoirs (melt sills), while the dominant lineation in the upper plutonic crust suggests vertically transported crystal-bearing melts or mushes. This is consistent with crystal-laden melts or mushes subsiding from the AML, and/or the crystallizing of upward migrating melts or mushes. For our petrological modeling we chose the first option, for the following reasons: (a) results from field studies in the Oman ophiolite using crystallographic preferred orientations imply crystal mushes subsiding from the AML down into the lower crust (e.g., Morales et al., 2011; Nicolas et al., 2009), in accord with a gabbro glacier mechanism. (b) This conclusion is consistent with the results from Pito Deep at EPR based on the analysis of microstructures (Brown et al., 2019) and of the magnetic structure (S. M. Maher et al., 2021). (c) In some varitextured gabbros we found minerals with very primitive cores, implying that primitive, parental melts are transported up to the AML, which can be regarded as the starting point for differentiation at the highest level in the plutonic crust, subsequently followed by downward movement of differentiated material in the form of a gabbro glacier, driven by hydrothermal cooling from above. (d) From the estimated pressures of crystallization from MORB basalts from fast-spreading ridges, Wanless and Shaw (2012) concluded that most crystallization occurs within the AML (75%), thus pointing to the dominant role of the AML as the locus for differentiation.

Thus, for the COMAGMAT modeling of the processes in the UFL and DGT we started at the top of our profile, with the same system composition as used for establishing the differentiation paths within the lower gabbros, and simulated downward differentiation. For this, we introduced a few intermediate differentiation steps and matched some of the natural compositions as shown in Figures 12a and 12b, which indicates that this procedure could be a reliable option. Data points in the plots which are more differentiated (left of the path in Figures 12a and 12b) could be due to in-situ crystallization, which is a common phenomenon in varitextured gabbros (Koepke et al., 2011; Müller et al., 2017). Data points which are less differentiated (right of the path in Figures 12a and 12b) could be interpreted as early crystallized products from fresh melts delivered from below. It should be noted that AMLs are transient, dynamic phenomena, which can move up and down during the lifetime of an

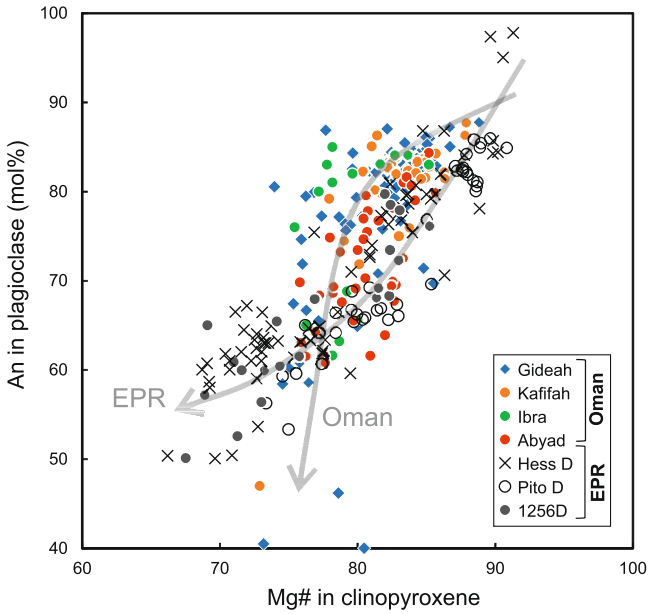

Figure 13. Chemical mineral evolution expressed by An content in plagioclase versus Mg# in clinopyroxenes of gabbros from the Oman ophiolite and from EPR crust. The data for Oman are the same as those used in Figure 11 (for references see caption of Figure 11). The data for Hess Deep are from Dick and Natland (1996), Miller et al. (1996), Natland and Dick (1996), and Lissenberg et al. (2013); those from Pito Deep are from Perk et al. (2007), and Constantin et al. (1996). Data from IODP Hole 1256D are from Koepke et al. (2011). The included differentiation paths are drawn by eye. For details see text.

active region of the axis of fast-spreading ridges (France et al., 2009; Zhang et al., 2014). It is important to emphasise that this is a very simple approach, with the only purpose to show that the proposed differentiation scenario for the UFL and DGT is an option. The scatter in the natural data for UFL and DGT is considerable, and the suggested path are very far from matching the scatter in the data.

COMAGMAT is able to predict the Mg# of olivine and clinopyroxene and the An content of plagioclase, but not the contents of minor elements in clinopyroxene, such as TiO_2 and Na_2O, which could be regarded as another constraint, whether differentiation trends are reliable or not. In order to focus on the observed minor element trends in clinopyroxene, we simply mirrored the differentiation paths of Mg# in clinopyroxene and An in plagioclase (which are more or less identical), and copied them into the corresponding plots (Figures 12c and 12d). For fine adjustments of the paths, we widened the paths a little bit in the x direction, but did not change the direction of the paths. As can be obtained from these plots, the match between the differentiation paths and the natural concentrations of TiO_2 and Na_2O in clinopyroxene is quite good, implying that our COMAGMAT modeling could indeed image the real differentiation processes in the Oman paleocrust.

4.4. Differentiation Trends for the Oman Paleocrust and for Recent EPR

Differentiation paths expressed by An content in plagioclase versus Mg# in clinopyroxenes from gabbros are plotted for available mineral data both from sites located in the Oman ophiolite (data are the same as those used in Section 4.2) and from modern EPR crust (Figure 13). Here data are available from Hess Deep (Dick & Natland, 1996; Lissenberg et al., 2013; Miller et al., 1996; Natland & Dick, 1996), from Pito Deep (Constantin et al., 1996; Perk et al., 2007), and from IODP Hole 1256D (Koepke et al., 2011). In spite of the broad scattering of the data, different evolution trends for both areas are visible, as shown in Figure 13. While the EPR sample suites follows straight evolution trends similar to those from other modern ridges (see compilation from Coogan, 2014), the trend for the Oman paleo ridge lower crust evolution shows in general higher An contents in plagioclase for a given Mg# in clinopyroxene, at least at the main stage of crystallization, implying higher water activities in the parental melts forming the Oman paleo ridge. However, the Oman trend is significantly different from evolution trends of typical arc gabbros, where the enrichment in An content is much stronger, as demonstrated in Kvassnes et al. (2004) for gabbros from the Troodos ophiolite or from the Izu-Bonin-Mariana fore-arc. This again emphasizes, as concluded above, that the magmatic processes which formed the Oman paleo ridge share more similarities with those active at modern fast-spreading mid-ocean ridges, than with those related to modern arc crust formation.

4.5. Hybrid Formation of the Lower Oceanic Crust in the Wadi Gideah

As shown in Section 4.3, the mineral evolutionary trends with crustal height imply different modi for the magmatic accretion of the Oman paleocrust; in-situ crystallization of individual melt sills coupled with upward differentiation for the lower two thirds of the crust (Layered Gabbro Unit and LFG), and downward transport of (crystal-laden) melts originating from the AML for the upper third (UFG and DGT). Our mineral data for the lower part of our transect clearly show an upward evolutionary trend (Figure 12), which is in accord with the sheeted sill accretion model (Kelemen et al., 1997), but not with a downward transported crystal/melt suspension originated from the AML (gabbro glacier), for which straight vertical evolutionary paths with constant compositions are predicted (see Figure 17 in Teagle et al., 2012). This emphasizes the importance of further melt lenses below the AML in the deeper crust under fast-spreading ridges. As cited in Section 1.1, meanwhile, several studies based on seismic experiments performed at fast- and intermediate-spreading ridges (EPR and Juan de Fuca Ridge) have been published, evidencing the presence of deep melt lenses under the ridges.

Reliable quantification of the number of sill injections in the lower crust is not available yet. Rough estimations are provided from high resolution investigations of the GT1 core from the OmanDP drilled in Wadi Gideah, where the results of the structural geology reveal thicknesses of coherent gabbro sections of about 30–50 m (based on the dip of the magmatic foliation; Kelemen et al., 2020). In the same core Mock, Axford Neave, et al. (2021) performed a high resolution phase analysis study, defining cycles of differentiation indicating an average thickness of several decameters per cycle. Finally, dimensions from individual melt reservoirs can be obtained from gabbro sills within the mantle below the crust, which range from ∼1 m to several decameters in size (e.g., Korenaga & Kelemen, 1997). But all these estimations are based on relatively primitive cumulate rocks, which were accumulated by poorly understood layer formation processes, with a high amount of liquid, which moved upward in a highly dynamic system. So the initial thickness of the melt lens remains unconstrained as of today. For stacked deep magma lenses in the plutonic crust at the Juan de Fuca Ridge which were investigated using seismic experiments, Carbotte et al. (2021) recently estimated a maximum thickness of the observed melt reservoirs of 140–170 m.

The only ∼160 m thick MTZ in the Wadi Gideah profile records extreme variations in the mineral compositions, showing the most primitive mineral data for olivine, clinopyroxene, and plagioclase, but also rather evolved compositions. These features are in strong contrast with the monotonous mineral trends of the 2.5 km layered gabbro above in the profile. In the MTZ, we recorded the highest density, by far, of different lithologies per volume as demonstrated in Figures 2g and 2h, where we present layered sequences on the dm to m scale of alternating olivine gabbros, dunites, troctolites, anorthosites, and wehrlites. These observations imply that the transition between crust and mantle is a special horizon, probably generating a permeability barrier (Korenaga & Kelemen, 1997), that enables the pooling of parental melts, homogenization, and crystallization before ascent into the overlying crust (e.g., Wanless & Shaw, 2012; Coogan, Gillis, et al., 2002). The presence of coherent wehrlite layers we observed in this horizon (Figures 2g and 2h) can be explained by locally higher water activities in the parental melt reservoirs, suppressing plagioclase in order to favor the wehrlitic paragenesis (olivine and clinopyroxene, without plagioclase; for details see Koepke, Feig, et al., 2021). This process was experimentally verified at a pressure of 200 MPa, corresponding to the base of the ocean crust (Koepke et al., 2009). The wehrlitic paragenesis is stabilized by pressure, which is probably the reason that wehrlites do not play a role in the layered gabbro series above (for details see Koepke, Feig, et al., 2021). Another peculiarity of this zone is that some mineral compositions are rather evolved providing evidence that relatively advanced differentiation stages are reached locally, which are not observed upward in the 2.5 km long sequence of monotonous layered gabbros (except for the crustal height at 2,139 m H.a.M, where oxide gabbros occur; see Section 4.3).

The magmatic accretion processes in the upper third of the plutonic crust (UFG and DGT) are quite different. A key observation is the record of very primitive compositions as relictic cores found in clinopyroxene and plagioclase crystals from gabbros of the DGT. Since these have been found in the varitextured gabbro which are regarded as frozen fillings of AMLs (e.g., Coogan, Thompson, & MacLeod, 2002; France et al., 2009; Koepke et al., 2011; Müller et al., 2017), we assume that differentiation starts within the AML at the top of the gabbroic crust. The importance of these melt reservoirs as sites for differentiation is also emphasized by the investigation of melt inclusions in olivines from MORBs recovered at fast- and intermediate-spreading ridges, showing that ∼75% of crystallization occurs here (Wanless & Shaw, 2012).

It should be noted that typical varitextured gabbros contain both relatively primitive poikilitic domains, where highly primitive mineral relics have been found, and rather differentiated granular domains in the interstices between the poikilitic clinopyroxenes, resulting in considerable spread of mineral compositions even within a given thin section. This is demonstrated in sample OM10-A12-1d, where the poikilitic domains reveal An contents in plagioclases from 76.6 to 60.3 mol%, while the granular domains show An contents from 69.7 to 21.08 mol%. This implies that the AMLs are sites where primitive melts mix with highly differentiated melts (Koepke et al., 2011; MacLeod & Yaouancq, 2000; Müller et al., 2017), which is the reason for the extreme heterogeneities recorded in these gabbros. From the AML horizon, sandwiched between the sheeted dikes and the uppermost gabbros, very heterogeneous masses, consisting of highly zoned accumulated crystals and differentiated interstitial melt, started to move downward as crystal-laden melts or more viscous mushes; this scenario is also supported by studies on microstructures of upper Oman gabbros (e.g., Morales et al., 2011; Nicolas et al., 2009). For the varitextured gabbros of the Wadi Gideah transect analyzed by EBSD, Mock, Ildefonse, et al. (2021) found, along with gabbros showing no preferred crystal orientation, gabbros indicating crystallization during a vertical flow, which we

interpreted as downward flow. During the downward flow the mushes may interact with mushes from previously active AMLs or with upward moving, more primitive parental melts, providing different modes of modification and assimilation, which leads to the large spread in mineral compositions observed within the UFL and DGT (Figure 9). The downward flow of crystal mush stops at the boundary between UFG and LFG, where the downward glacier flux meets the upward flowing mushes originated by melt sill injections.

Our findings are inconsistent with purely topdown crystal/melt suspensions forming the lower crust ("gabbro glacier model", e.g., Henstock et al., 1993; Quick & Denlinger, 1993). Instead we favor a hybrid model for crustal accretion with injection of melt sills and in-situ crystallization in the lower part of the crust, and significant crystallization in the AML followed by a downward crystal/melt suspension. Thus, this model combines the two endmember models.

Accretion models based on two different mechanisms have also been published in the past; Kelemen et al. (1997) and Boudier et al. (1996) both show differences compared to the model presented here. The former authors also include a downward mush flow from the AML, but regarded this zone as relatively thin (a few hundred meters below the AML), while this study emphasizes the importance of the gabbro glacier process for the uppermost 1500 m below the AML. Boudier et al. (1996) suggested a hybrid accretion model 25 years ago. The characteristic feature of their model is that sill injections are distributed within a gabbro glacier that expands over the entire plutonic crust. In the model presented here, however, the downward flow of crystal/melt suspensions is restricted to the upper 1.5 km of the plutonic crust only (UFG and DGT), while in the 3.5 km below we favor a pure sill injection process.

Our hybrid model presented here, is also in contrast with the "full sheeted sill" model presented in the recent paper of VanTongeren et al. (2021), where a model is presented that the whole plutonic crust was formed via *in situ* crystallization. One aspect of their study is that their group of upper gabbros (uppermost 1500 m) which is regarded as more evolved compared to the lower gabbros, consists of only four samples. In the corresponding downhole plot for clinopyroxene, only four data points are plotted, with two, which are as primitive as those from the layered gabbros below, and two, which are more evolved. Thus, the spread of data is similar with that for the upper gabbros from the Wadi Gideah in this study, but the number of samples is probably too low for any significant conclusion on the accretion process, compared to the 22 samples for the upper gabbros (UFG and DGT) used in this study. On the other hand, our hybrid model is in accord with the findings of S. M. Maher et al. (2021) from Pito Deep, who investigated the magnetic structure of gabbro samples collected by a remote objected vessel (ROV) up to a depth of 1 km below the dike/gabbro contact. These authors conclude that the uppermost gabbros have been formed under conditions of conducting cooling, implying a gabbro glacier flow as process of accretion.

In spite of the very close similarity in formation processes between EPR and the Oman magmatic Phase 1 paleoridge, it should be emphasized that a significant difference exists with respect to the water content of the parental melts. While the EPR parental melts are regarded as dry, those forming the magmatic Phase 1 paleoridge have been hydrous, as shown by the COMAGMAT modeling in Section 4.3. The plagioclase evolutionary trend of the natural rocks can be adequately reproduced with an initial water content of 0.8 wt%. In addition to the initial water content values in the parental melts of MacLeod et al. (2013), who estimated 0.2–1 wt% based on MELTS modeling for the extrusive V1 sequence ("Geotimes" lavas), we now have a second robust value, derived independently by modeling with COMAGMAT, for a completely different lithology making up the lower part of the Oman paleo crust. For this, we focused in our modeling on reproducing the plagioclase composition recorded in our profile, since the An content in plagioclase is most sensitive to varying water activities in silicate melt.

Elevated water content in the parental melts is also indicated by the slight inverse zoning in plagioclase from the Layered Gabbro Unit and the LFG, which is shown by 85% of those rim/core pairs which passed the *t*-test (25 pairs; Figure 10a). This effect can be explained by small enrichments of the water in the residual melts due to slight differentiation effects, since the strong dependence of An content on the water activity is experimentally well verified by numerous studies (e.g., Berndt et al., 2005; Feig et al., 2006; Gaetani et al., 1993). Slightly positive rim/core values for TiO_2 and negative values for Cr_2O_3 in clinopyroxene support this model, and argue against a model that suggests that the enrichment of An in the rims is due to replenishment with more primitive melts. The trend for the inverse zonation of plagioclase is reversed when entering the UFG and DGT. Here, the much stronger differentiation leads to significantly lower Ca/Na ratios, which overcompensates for the increasing water content in the residual melts. It should be noted that zoning in clinopyroxene, especially in the lower

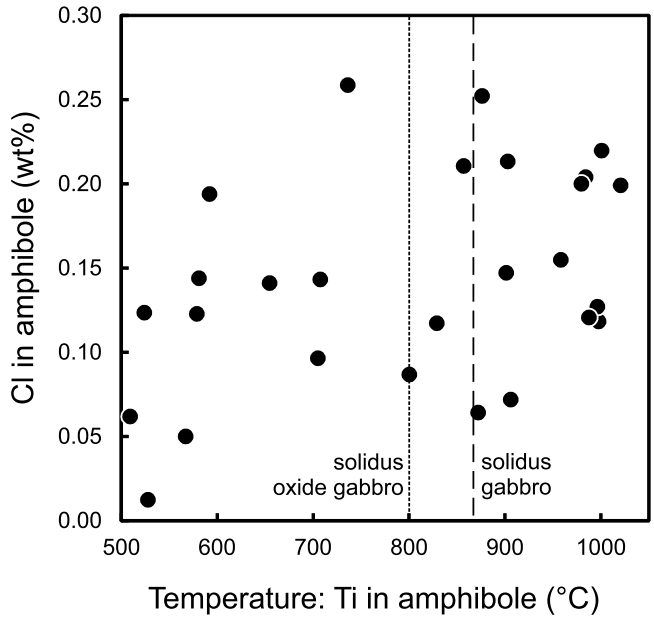

Figure 14. Cl concentrations versus formation temperature of amphiboles from those gabbros influenced by HTFZs. Petrographic details can be obtained from Table S3 in Supporting Information S1 (PANGAEA data repository; Koepke, Garbe-Schönberg, et al., 2021). Only those amphiboles are considered which have been characterized as magmatic by petrographic inspection. Those amphiboles with low formation temperatures derived by the semiquantitative Ti-in-amphibole geothermometer (Ernst & Liu, 1998) are influenced by secondary alteration. The wet solidi for oxide gabbros and for gabbros (including olivine gabbros) are from Koepke et al. (2018) and Koepke et al. (2004), respectively.

crust, is in general low, and is much less developed than the zoning effects reported by Lissenberg et al. (2013) for the gabbros from Hess Deep at the EPR, implying that reactive porous flow in the Oman paleo crust played only a minor role.

4.6. The Role of Hydrothermal Fault Zones for the Cooling of the Deep Crust

A requirement for our hybrid model is significant hydrothermal cooling close to the ridge axis in the lower crust for the consumption of the latent heat of crystallization. This is also supported by thermal models for the cooling of fast-spreading oceanic crust (e.g., Maclennan et al., 2005; Theissen-Krah et al., 2011, 2016). In principle, cooling rates estimated for the complete oceanic crust could play a key role in unraveling the different mechanisms of crustal accretion. However, several studies on the quantification of cooling rate by different techniques obtained rather different results which are difficult to reconcile and which do not provide an unambiguous answer on how the lower crust is formed under fast-spreading systems (e.g., Coogan, Jenkin, & Wilson, 2002; Dygert et al., 2017; Faak & Gillis, 2016; Garrido et al., 2001; Schmitt et al., 2011; Sun & Lissenberg, 2018; VanTongeren et al., 2008; Zhang et al., 2014).

Based on a new profile through the Oman paleocrust with high spatial resolution, we present in this study strong evidence for in-situ crystallization of the lower crust, which calls for a deep cooling system enabling crystallization. In this context, we emphasize the role of HTFZs, which have the potential for transporting focused, seawater-derived fluids into the deep crust (e.g., Coogan et al., 2006; Zihlmann et al., 2018), in order to establish cooling. For one zone located in the layered gabbros at a crustal height of 1092 m H.a.M that was investigated in detail by Zihlmann et al. (2018), it was shown by mass balance calculation that such a fault zone may contribute considerably to the global hydrothermal budgets for many elements. Moreover, these authors concluded that the contribution of such zones to global hydrothermal fluxes is significant. While the mineral compositions and parageneses studied in HTFZ rocks by Coogan et al. (2006) and Zihlmann et al. (2018) recorded temperatures mainly in the greenschist and amphibolite facies, our study sheds new light on the initial temperatures of such zones, suggesting magmatic conditions. This is indicated both by the presence of magmatic veins and by the occurrence of hornblende-bearing rocks cutting the layered gabbros in several places (see Sections 3.2.5 and 3.3.2).

Of special interest are microstructures in a gabbro in the large HTFZ at the crustal height of 1205 m H.a.M., indicating that hydrous partial melting occurred on grain boundaries (sample OM12-27; Figure 7). These microstructures, together with the compositional record in the newly formed mineral phases (An-rich plagioclase, pargasitic amphibole, ± orthopyroxene), imply that water-rich fluids percolated between the grains, as explained in detail in Section 3.3.2. Provided that these fluids are seawater derived, these hydrous partial melting microstructures provide strong evidence that initial cooling occurred via a fluid veining system, which was active during the on-axis phase of the ridge, where magmatic processes dominated.

Crucial evidence that the involved fluids were related to seawater came from the chemistry of brown hornblendes occurring in these rocks related to HTFZs. Many of them, mostly of pargasitic compositions, show high chlorine contents (up to 0.25 wt%) with those values typical for experimental amphiboles grown in a melt with high chlorine activity as shown in Figure 14, implying seawater/rock interaction under magmatic conditions. This figure also verifies that many of the analyzed amphiboles show formation temperatures above the wet gabbro solidus (up to 1020°C), which were calculated with the help of the semiquantitative Ti-in-amphibole geothermometer (Ernst & Liu, 1998). The analyses are presented in Table S3 in in Supporting Information S1 (PANGAEA data repository; Koepke, Garbe-Schönberg, et al., 2021).

It should be noted that other studies from Oman also reported the initiation of hydrothermal cooling in the deep crust at very high temperatures, up to the magmatic regime. Nicolas et al. (2003) observed a thermally induced microcrack network cutting deep layered gabbros in which very high mineral formation temperatures have been recorded. Isotope investigations on the mineralogical fillings of these cracks revealed seawater-derived hydrothermal fluids (Bosch et al., 2004). Moreover, Abily et al. (2011) observed the presence of deep, synmagmatic normal faults in the lowermost gabbros from the Sumail massif in the Oman ophiolite, with the potential to transport hydrothermal fluid deep into the crust catalyzing a wet magmatism.

Our observations imply that the initiation of the hydrothermal vein system in such fault zones is established on-axis under magmatic conditions. Later, in an advanced cooling stage, the same pathways were used at lower temperatures for pervasive alteration in the amphibolite and greenschist facies, as indicated by relics of magmatic brown hornblende in some wall rocks, fault rocks, or metagabbros sampled in HTFZs. To evaluate the potential of cooling the lower crust by such fault zones more investigations are necessary, including a careful, systematic mapping and a reasonably dense sampling of such HTFZs, as well as advanced geochemical and isotope geochemical work in order to estimate mass balance calculations and to quantify the interaction with seawater-derived hydrothermal fluids, active during the phase of oceanic spreading.

However, from our petrological modeling it is questioned, whether such a hydrothermal cooling system is really needed for removing the latent heat of crystallization of the deep crust under fast-spreading ridges, since the fraction of crystals is only small: the median for those fractionation steps involved in simulating the crystallization of the layered gabbros in our profile, is only 4.0 mol%. In contrast, full crystallization of deep melt lenses is assumed in those thermal models related to the sheeted sill model. This implies that the upmoving melts could easily transport the additional heat produced by deep crystallization, upward. The main crystallization then follows in the AML, where, according to Wanless and Shaw (2012), 75% of the crystallization at fast-spreading ridges occur. The very low grade of crystallization is also in accord with the observation from the petrography that the layered gabbros are rocks lacking late-stage crystallization, which is in strong contrast to deep gabbros from slow-spreading ridges, where late-stage crystallization is ubiquitous. Future studies with more sophisticated modeling involving also mass balance and with focus on high spatial resolution isotopic analyses on minerals (Lambart et al., 2019) will shed more light on the complex process of cumulate formation under fast-spreading mid-ocean ridges.

5. Conclusions

A reference profile through fast-spreading lower oceanic crust was established by outcrop sampling in the Wadi Gideah and surroundings, which consists of 465 samples from the mantle, through gabbros up to the DGT. A special feature of this profile is that identical samples have been analyzed by several quite different methods: mineral major and trace element chemistry, bulk rock geochemistry, isotope geochemistry, and EBSD. In this study we present results obtained by petrography and petrology.

Depth profiles of mineral compositions combined with petrological modeling reveal insights into the mode of magmatic formation of fast-spreading lower oceanic crust, implying a hybrid accretion mechanism. The lower two thirds of the gabbroic crust (Layered Gabbro Unit and LFG), formed via the injection of melt sills and in situ crystallization. Here, upward moving fractionated melts mixed with more primitive melts through melt replenishments, resulting in a slight but distinct upward differentiation trend. The upper third of the gabbroic crust (UFG and DGT) is significantly more differentiated, in accord with a model of downward differentiation of a primitive parental melt originated from the AML located at the top of the gabbroic crust.

We emphasize the close similarity in the magmatic processes between the Oman paleoridge and the modern EPR, when considering only the products of magmatic Phase 1 for the Oman case, except for one parameter; the water content of the parental MORB melts. While the parental MORB melts of the EPR are regarded as dry, the melts which generated the Oman paleo crust were hydrous, with an estimated water content of ∼0.8 wt%, due to the tectonic setting of subduction zone initiation.

We emphasize the importance of deep HTFZs, initially formed on-axis at very high temperatures in the magmatic regime. Relics of magmatic hornblende formed at that high-temperature stage observed in magmatic veins within

gabbros, in the wall rocks and in metagabbros of the HTFZs imply that the same pathways have been used later for pervasive off-axis alteration mostly in the greenschist facies.

Data Availability Statement

The data obtained for this study and discussed in this study will be available on the FAIR-aligned PANGAEA data repository (Koepke, Garbe-Schönberg, et al., 2021).

Acknowledgments
This work would not have been possible without the help of Adolphe Nicolas and Francoise Boudier during an initial state of the project. The authors wish to thank Otto Dietrich and J. Feige for careful thin section preparation. The friendly cooperation established in Oman with the Public Authority for Mining (Department of Geological Research, Dr. A. Al Rajhi and Dr. M. Alaraimi) is acknowledged. This study was funded by projects KO 1723/16-1, KO 1723/21-1, and KO 1723/25-1 of the Deutsche Forschungsgemeinschaft (DFG) within the priority program SPP 1006: ICDP. Open access funding enabled and organized by Projekt DEAL.

References

Abily, B., Ceuleneer, G., & Launeau, P. (2011). Synmagmatic normal faulting in the lower oceanic crust: Evidence from the Oman ophiolite. *Geology*, *39*(4), 391–394. https://doi.org/10.1130/g31652.1

Alt, J. C., Laverne, C., Vanko, D., Tartarotti, P., Teagle, D. A. H., Bach, W., et al. (1996). Hydrothermal alteration of a section of upper oceanic crust in the eastern equatorial Pacific: A synthesis of results from DSDP/ODP legs 69, 70, 83, 111, 137, 140, 148 at site 504B. *Proceedings of the Ocean Drilling Program, Scientific Results*, *148*, 417–434.

Ariskin, A., & Barmina, G. (2004). COMAGMAT: Development of a magma crystallization model and its petrological applications. *Geochemistry International*, *42*(Suppl. 1), S1–S157.

Bedard, J. H., Sparks, R. S. J., Renner, R., Cheadle, M. J., & Hallworth, M. A. (1988). Peridotite sills and metasomatic gabbros in the Eastern layered series of the Rhum complex. *Journal of the Geological Society*, *145*, 207–224. https://doi.org/10.1144/gsjgs.145.2.0207

Belgrano, T. M., Diamond, L. W., Vogt, Y., Biedermann, A. R., Gilgen, S. A., & Al-Tobi, K. (2019). A revised map of volcanic units in the Oman ophiolite: Insights into the architecture of an oceanic proto-arc volcanic sequence. *Solid Earth*, *10*, 1181–1217. https://doi.org/10.5194/se-10-1181-2019

Berndt, J., Koepke, J., & Holtz, F. (2005). An experimental investigation of the influence of water and oxygen fugacity on differentiation of MORB at 200 MPa. *Journal of Petrology*, *46*(1), 135–167.

Bosch, D., Jamais, M., Boudier, F., Nicolas, A., Dautria, J.-M., & Agrinier, P. (2004). Deep and high-temperature hydrothermal circulation in the Oman ophiolite - Petrological and isotopic evidence. *Journal of Petrology*, *45*, 1181–1208. https://doi.org/10.1093/petrology/egh010

Boudier, F., Nicolas, A., & Ildefonse, B. (1996). Magma chambers in the Oman ophiolite: Fed from the top and the bottom. *Earth and Planetary Science Letters*, *144*(1–2), 239–250. https://doi.org/10.1016/0012-821x(96)00167-7

Brown, T., Cheadle, M., John, B., Coogan, L., Gee, J., Karson, J. A., & Swapp, S. (2019). Textural character of gabbroic rocks from Pito deep: A record of magmatic processes and the genesis of the upper plutonic crust at fast-spreading mid-ocean ridges. *Journal of Petrology*, *60*(5), 997–1026. https://doi.org/10.1093/petrology/egz022

Browning, P. (1982). *The petrology, geochemistry, and the structure of the plutonic rocks of the Oman ophiolite*. (PhD Thesis). Open University.

Browning, P. (1984). Cryptic variation within the cumulate sequence of the Oman ophiolite: Magma chamber depth and petrological implications. *Geological Society, London, Special Publications*, *13*(1), 71–82. https://doi.org/10.1144/gsl.Sp.1984.013.01.07

Canales, J. P., Detrick, R. S., Toomey, D. R., & Wilcock, W. S. D. (2003). Segment-scale variations in the crustal structure of 150-300 kyr old fast spreading oceanic crust (East Pacific Rise, 8°15′N-10°5′N) from wide-angle seismic refraction profiles. *Geophysical Journal International*, *152*, 766–794. https://doi.org/10.1046/j.1365-246x.2003.01885.x

Canales, J. P., Nedimovic, M. R., Kent, G. M., Carbotte, S. M., & Detrick, R. S. (2009). Seismic reflection images of a near-axis melt sill within the lower crust at the Juan de Fuca ridge. *Nature*, *460*(7251), 89–U100. https://doi.org/10.1038/nature08095

Cannat, M. (1996). How thick is the magmatic crust at slow spreading oceanic ridges? *Journal of Geophysical Research*, *101*, 2847–2857. https://doi.org/10.1029/95jb03116

Carbotte, S. M., Canales, J. P., Nedimovic, M. R., carton, H., & Mutter, J. C. (2012). Recent seismic studies at the East Pacific Rise 8°20′-10°10′ and Endeavour Segment: Insight into mid-ocean ridge hydrothermal and matmatic processes. *Oceanography*, *25*, 100–112. https://doi.org/10.5670/oceanog.2012.08

Carbotte, S. M., Marjanović, M., Arnulf, A. F., Nedimović, M. R., Canales, J. P., & Arnoux, G. M. (2021). Stacked magma lenses beneath mid-ocean ridges: Insights from new seismic observations and synthesis with prior geophysical and geologic findings. *Journal of Geophysical Research: Solid Earth*, *126*(4), e2020JB021434. https://doi.org/10.1029/2020jb021434

Christie, D. M., Ildefonse, B., Abe, N., Arai, S., Bach, W., Blackman, D. K., et al. (2006). Mission Moho: Formation of oceanic lithosphere. *Eos*, *87*, 539. https://doi.org/10.1029/2006eo480005

Constantin, M., Hékinian, R., Bideau, D., & Hébert, R. J. (1996). Construction of the oceanic lithosphere by magmatic intrusions: Petrological evidence from plutonic rocks formed along the fast-spreading East Pacific Rise. *Geology*, *24*(8), 731–734. https://doi.org/10.1130/0091-7613(1996)024<0731:cotolb>2.3.co;2

Coogan, L. A. (2014). The lower oceanic crust. In K. Turekian, & H. D. Holland (Eds.), *Treatise on geochemistry* (2nd ed., pp. 497–541). Elsevier. https://doi.org/10.1016/b978-0-08-095975-7.00316-8

Coogan, L. A., Gillis, K. M., MacLeod, C. J., Thompson, G. M., & Hekinian, R. (2002). Petrology and geochemistry of the lower ocean crust formed at the East Pacific Rise and exposed at Hess deep: A synthesis and new results. *Geochemistry, Geophysics, Geosystems*, *3*. https://doi.org/10.1029/2001GC000230

Coogan, L. A., Howard, K. A., Gillis, K. M., Bickle, M. J., Chapman, H., Boyce, A. J., et al. (2006). Chemical and thermal constraints on focussed fluid flow in the lower oceanic crust. *American Journal of Science*, *306*(6), 389–427. https://doi.org/10.2475/06.2006.01

Coogan, L. A., Jenkin, G. R. T., & Wilson, R. N. (2002). Constraining the cooling rate of the lower oceanic crust: A new approach applied to the Oman ophiolite. *Earth and Planetary Science Letters*, *199*(1–2), 127–146. https://doi.org/10.1016/s0012-821x(02)00554-x

Coogan, L. A., Thompson, G., & MacLeod, C. J. (2002). A textural and geochemical investigation of high level gabbros from the Oman ophiolite: Implications for the role of the axial magma chamber at fast-spreading ridges. *Lithos*, *63*(1–2), 67–82. https://doi.org/10.1016/s0024-4937(02)00114-7

de Graaff, S., Goodenough, K., Klaver, M., Lissenberg, C., Jansen, M., Millar, I., & Davies, G. (2019). Evidence for a moist to wet source transition throughout the Oman-UAE ophiolite, and implications for the geodynamic history. *Geochemistry, Geophysics, Geosystems*, *20*(2), 651–672. https://doi.org/10.1029/2018gc007923

Detrick, R. S., Buhl, P., Vera, E., Mutter, J., Orcutt, J., Madsen, J., & Brocher, T. (1987). Multichannel seismic imaging of a crustal magma chamber along the East Pacific Rise. *Nature*, *326*, 35–41. https://doi.org/10.1038/326035a0

Dick, H. J. B., & Natland, J. H. (1996). Late-stage melt evolution and transport in the shallow mantle beneath the East Pacific Rise. *Proceedings of the Ocean Distillation Program, Scientific Results*, *147*, 103–134. https://doi.org/10.2973/odp.proc.sr.147.007.1996

Dick, H. J. B., Natland, J. H., & Ildefonse, B. (2006). Deep drilling in the oceanic crust and mantle. *Oceanography*, *19*, 74–82. https://doi.org/10.5670/oceanog.2006.06

Dygert, N., Kelemen, P. B., & Liang, Y. (2017). Spatial variations in cooling rate in the mantle section of the Samail ophiolite in Oman: Implications for formation of lithosphere at mid-ocean ridges. *Earth and Planetary Science Letters*, *465*, 134–144. https://doi.org/10.1016/j.epsl.2017.02.038

Ernst, W. G., & Liu, J. (1998). Experimental phase-equilibrium study of Al- and Ti-contents of calcic amphibole in MORB - A semiquantitative thermobarometer. *American Mineralogist*, *83*, 952–969. https://doi.org/10.2138/am-1998-9-1004

Faak, K., & Gillis, K. M. (2016). Slow cooling of the lowermost oceanic crust at the fast-spreading East Pacific Rise. *Geology*, *44*(2), 115–118. https://doi.org/10.1130/g37353.1

Feig, S. T., Koepke, J., & Snow, J. E. (2006). Effect of water on tholeiitic basalt phase equilibria: An experimental study under oxidizing conditions. *Contributions to Mineralogy and Petrology*, *152*(5), 611–638. https://doi.org/10.1007/s00410-006-0123-2

France, L., Ildefonse, B., & Koepke, J. (2009). Interactions between magma and the hydrothermal system in the Oman ophiolite and in IODP hole 1256D: Fossilisation of a dynamic melt lens at fast spreading ridges. *Geochemistry, Geophysics, Geosystems*, *10*. https://doi.org/10.1029/2009GC002652

France, L., Lombard, M., Christian, N., Berthod, C., Debret, B., Koepke, J., et al. (2021). Quantifying the axial magma lens dynamics at the roof of oceanic magma reservoirs (Dike/Gabbro transition): Oman drilling project GT3 site Survey. *Journal of Geophysical Research: Solid Earth*, *126*. https://doi.org/10.1029/2020JB021496

Gaetani, G. A., Grove, T. L., & Bryan, W. B. (1993). The influence of water on the petrogenesis of subduction-related igneous rocks. *Nature*, *365*(6444), 332–334. https://doi.org/10.1038/365332a0

Garrido, C. J., Kelemen, P. B., & Hirth, G. (2001). Variation of cooling rate with depth in lower crust formed at an oceanic spreading ridge: Plagioclase crystal size distributions in gabbros from the Oman ophiolite. *Geochemistry, Geophysics, Geosystems*, *2*, 2000GC000136. https://doi.org/10.1029/2000gc000136

Gillis, K. M. (2008). The roof of an axial magma chamber: A hornfelsic heat exchanger. *Geology*, *36*(4), 299–302. https://doi.org/10.1130/g24590a.1

Gillis, K. M., Snow, J. E., Klaus, A., Abe, N., Adriao, A. B., Akizawa, N., et al. (2014). Primitive layered gabbros from fast-spreading lower oceanic crust. *Nature*, *505*(7482), 204–207. https://doi.org/10.1038/nature12778

Gillis, K. M., Snow, J. E., Klaus, J. E., & the Expedition 345 Scientists (2014). Expedition 345. Proceedings of the Integrated Ocean Drilling Program.

Godard, M., Dautria, J.-M., & Perrin, M. (2003). Geochemical variability of the Oman ophiolite lavas: Relationship with spatial distribution and paleomagnetic directions. *Geochemistry, Geophysics, Geosystems*, *4*, 2002GC000452. https://doi.org/10.1029/2002gc000452

Goodenough, K. M., Thomas, R. J., Styles, M. T., Schofield, D. I., & MacLeod, C. J. (2014). Records of ocean growth and destruction in the Oman-UAE ophiolite. *Elements*, *10*(2), 109–114. https://doi.org/10.2113/gselements.10.2.109

Gregory, R. T., & Taylor, H. P. (1981). An oxygen isotope profile in a section of Cretaceous oceanic crust, Semail ophiolite, Oman: Evidence for $d^{18}O$ buffering of the ocean by deep (>5 km) seawater hydrothermal circulation at mid-ocean ridges. *Journal of Geophysical Research*, *86*, 2737–2755. https://doi.org/10.1029/jb086ib04p02737

Henstock, T. J., Woods, A. W., & White, R. S. (1993). The accretion of oceanic crust by episodic sill intrusion. *Journal of Geophysical Research*, *98*(B3), 4143–4161. https://doi.org/10.1029/92jb02661

Holness, M. B. (2014). The effect of crystallization time on plagioclase grain shape in dolerites. *Contributions to Mineralogy and Petrology*, *168*(5), 1076. https://doi.org/10.1007/s00410-014-1076-5

Ildefonse, B., Abe, N., Kelemen, P., Kumagai, H., Teagle, D., Wilson, D., & Moho Proponents, M. (2009). Mission Moho: Rationale for drilling deep through the ocean crust into the upper mantle. *Paper presented at the EGU general assembly conference abstracts*.

Ishizuka, O., Tani, K., & Reagan, M. K. (2014). Izu-bonin-mariana forearc crust as a modern ophiolite analogue. *Elements*, *10*(2), 115–120. https://doi.org/10.2113/gselements.10.2.115

Juteau, T., Beurrier, M., Dahl, R., & Nehlig, P. (1988). Segmentation at a fossil spreading axis: The plutonic sequence of the Wadi Haymiliyah area (Haylayn Block, Sumail Nappe, Oman). *Tectonophysics*, *151*, 167–197. https://doi.org/10.1016/0040-1951(88)90245-4

Kelemen, P., Matter, J., Teagle, D., Coggon, J. & the Oman Drilling Project Science Team (2020). *Proceedings of the Oman drilling project*. International Ocean Discovery Program. https://doi.org/10.14379/OmanDP.proc.2020

Kelemen, P. B., Koga, K., & Shimizu, N. (1997). Geochemistry of gabbro sills in the crust-mantle transition zone of the Oman ophiolite: Implications for the origin of the oceanic lower crust. *Earth and Planetary Science Letters*, *146*(3–4), 475–488. https://doi.org/10.1016/s0012-821x(96)00235-x

Kinzler, R. J., & Grove, T. L. (1993). Corrections and further discussion of the primary magmas of midocean ridge basalts, 1 and 2. *Journal of Geophysical Research*, *98*(B12), 22339–22347. https://doi.org/10.1029/93jb02164

Koepke, J., Berndt, J., Horn, I., Fahle, J., & Wolff, P. E. (2014). Partial melting of oceanic gabbro triggered by propagating water-rich fluids: A prime example from the Oman ophiolite. In H. R. Rollinson, M. P. Searle, I. A. Abbasi, A. Al-Lazki, & M. H. Al-Kindi (Eds.), *Tectonic evolution of the Oman mountains* (pp. 187392–188204). Geological Society of London, Special Publication.

Koepke, J., Botcharnikov, R., & Natland, J. H. (2018). Crystallization of late-stage MORB under varying water activities and redox conditions: Implications for the formation of highly evolved lavas and oxide gabbro in the ocean crust. *Lithos*. https://doi.org/10.1016/j.lithos.2018.10.001

Koepke, J., Christie, D. M., Dziony, W., Holtz, F., Lattard, D., Maclennan, J., et al. (2008). Petrography of the dike/gabbro transition at IODP site 1256D (Equatorial Pacific): The evolution of the granoblastic dikes. *Geochemistry, Geophysics, Geosystems*, *9*. https://doi.org/10.1029/2008GC001939

Koepke, J., Feig, S. T., Berndt, J., Neave, D. A. & the Oman Drilling Project Science Team (2021). Wet magmatic processes during the accretion of the deep crust of the Oman Ophiolite paleoridge: Phase diagrams and petrological records. *Tectonophysics*, *817*, 229051. https://doi.org/10.1016/j.tecto.2021.229051

Koepke, J., Feig, S. T., & Snow, J. (2005). Late-stage magmatic evolution of oceanic gabbros as a result of hydrous partial melting: Evidence from the ODP leg 153 drilling at the mid-atlantic ridge. *Geochemistry, Geophysics, Geosystems*, *6*, 000801–000827, 2004GC000805. https://doi.org/10.1029/2004gc000805

Koepke, J., Feig, S. T., Snow, J., & Freise, M. (2004). Petrogenesis of oceanic plagiogranites by partial melting of gabbros: An experimental study. *Contributions to Mineralogy and Petrology*, *146*, 414–432. https://doi.org/10.1007/s00410-003-0511-9

Koepke, J., France, L., Müller, T., Faure, F., Goetze, N., Dziony, W., & Ildefonse, B. (2011). Gabbros from IODP Site 1256 (Equatorial Pacific): Insight into axial magma chamber processes at fast-spreading ocean ridges. *Geochemistry, Geophysics, Geosystems*, *12*. https://doi.org/10.1029/2011GC003655

Koepke, J., Garbe-Schönberg, D., Müller, T., Mock, D., Müller, S., & Nasir, S. (2021). A reference section through fast-spread lower oceanic crust, Wadi Gideah, Samail ophiolite (Sultanate of Oman): Petrographic data table and mineral analyses performed by EPMA. *PANGAEA*. https://doi.org/10.1594/PANGAEA.939358

Koepke, J., Schoenborn, S., Oelze, M., Wittmann, H., Feig, S., Hellebrand, E., et al. (2009). Petrogenesis of crustal wehrlites in the Oman ophiolite: Experiments and natural rocks. *Geochemistry, Geophysics, Geosystems*, *10*. https://doi.org/10.1029/2009GC002488

Koepke, J., & Zhang, C. (2021). Axial melt lens dynamics at fast-spreading mid-ocean ridges. In F. Vetere (Ed.), *Dynamic magma evolution* (Vol. 254). (ISBN: 978-1-119-52113-6). AGU Geophysical Monograph.

Korenaga, J., & Kelemen, P. B. (1997). Origin of gabbro sills in the Moho transition zone of the Oman ophiolite: Implications for magma transport in the oceanic lower crust. *Journal of Geophysical Research*, *102*(B12), 27729–27749. https://doi.org/10.1029/97jb02604

Kvassnes, A. J. S., Strand, A. H., Moen-Eikeland, H., & Pedersen, R. (2004). The Lyngen Gabbro: The lower crust of an Ordovician Incipient arc. *Contributions to Mineralogy and Petrology*, *148*, 358–379. https://doi.org/10.1007/s00410-004-0609-8

Lambart, S., Koornneef, J. M., Millet, M. A., Davies, G. R., Cook, M., & Lissenberg, C. J. (2019). Highly heterogeneous depleted mantle recorded in the lower oceanic crust. *Nature Geoscience*, *12*, 482–486. https://doi.org/10.1038/s41561-019-0368-9

Lissenberg, C. J., MacLeod, C. J., Howard, K. A., & Godard, M. (2013). Pervasive reactive melt migration through fast-spreading lower oceanic crust (Hess Deep, equatorial Pacific Ocean). *Earth and Planetary Science Letters*, *361*, 436–447. https://doi.org/10.1016/j.epsl.2012.11.012

Lofgren, G. E., & Donaldson, C. H. (1975). Curved branching crystals and differentiation in comb-layered rocks. *Contributions to Mineralogy and Petrology*, *49*, 309–319. https://doi.org/10.1007/bf00376183

Maclennan, J., Hulme, T., & Singh, S. C. (2004). Thermal models of oceanic crustal accretion: Linking geophysical, geological and petrological observations. *Geochemistry, Geophysics, Geosystems*, *5*, 2003GC000605. https://doi.org/10.1029/2003gc000605

Maclennan, J., Hulme, T., & Singh, S. C. (2005). Cooling of the lower oceanic crust. *Geology*, *33*, 357–360. https://doi.org/10.1130/g21207.1

MacLeod, C. J., Johan Lissenberg, C., & Bibby, L. E. (2013). Moist MORB" axial magmatism in the Oman ophiolite: The evidence against a mid-ocean ridge origin. *Geology*, *41*(4), 459–462. https://doi.org/10.1130/g33904.1

MacLeod, C. J., & Yaouancq, G. (2000). A fossil melt lens in the Oman ophiolite: Implications for magma chamber processes at fast spreading ridges. *Earth and Planetary Science Letters*, *176*, 357–373. https://doi.org/10.1016/s0012-821x(00)00020-0

Maher, S., Gee, J., Doran, A., Cheadle, M., & John, B. (2020). Magnetic structure of fast-spread oceanic crust at Pito Deep. *Geochemistry, Geophysics, Geosystems*, *21*(2), e2019GC008671. https://doi.org/10.1029/2019gc008671

Maher, S. M., Gee, J. S., Cheadle, M. J., & John, B. E. (2021). Three-dimensional magnetic stripes require slow cooling in fast-spread lower ocean crust. *Nature*, *597*, 511–515. https://doi.org/10.1038/s41586-021-03831-6

Marjanovic, M., Carbotte, S. M., Carton, H., Nedimovic, M. R., Mutter, J. C., & Canales, J. P. (2014). A multi-sill magma plumbing system beneath the axis of the East Pacific Rise. *Nature Geoscience*, *7*(11), 825–829. https://doi.org/10.1038/ngeo2272

McCulloch, M. T., Gregory, R. T., Wasserburg, G. J., & Taylor, H. P. (1981). Sm-Nd, Rb-Sr, and $^{18}O/^{16}O$ systematics in an oceanic crustal section: Evidence from the Samail ophiolite. *Journal of Geophysical Research*, *86*(B4), 2721–2735. https://doi.org/10.1029/jb086ib04p02721

Miller, D. J., Iturrino, G. J., & Christensen, N. I. (1996). Geochemical and petrological constraints on velocity behavior of lower crustal and upper mantle rocks from the fast-spreading ridge at Hess Deep. *Proceedings of the Ocean Drilling Project, Scientific Results*, *147*, 477–490. https://doi.org/10.2973/odp.proc.sr.147.028.1996

Mock, D., Axford Neave, D., Müller, S., Garbe-Schönberg, D., Ildefonse, B., & Koepke, J. (2021). Accretion of fast-spread lower oceanic crust: Drill core GT1 from the ICDP Oman drilling project. *Paper presented at the EGU general assembly conference abstracts*.

Mock, D., Ildefonse, B., Müller, T., & Koepke, J. (2021). A reference section through fast-spread lower oceanic crust, Wadi Gideah, Samail ophiolite (Sultanate of Oman): Insights from crystallographic preferred orientations. *Journal of Geophysical Research: Solid Earth*, e2021JB021864. https://doi.org/10.1029/2021jb021864

Mock, D., Neave, D., Müller, S., Garbe-Schönberg, D., Namur, O., Ildefonse, B., & Koepke, J. (2020). Formation of igneous layering in the lower oceanic crust from the Samail Ophiolite, Sultanate of Oman. *Journal of Geophysical Research: Solid Earth*, e2020JB019573.

Morales, L. F. G., Boudier, F., & Nicolas, A. (2011). Microstructures and crystallographic preferred orientation of anorthosites from Oman ophiolite and the dynamics of melt lenses. *Tectonics*, *30*(2). https://doi.org/10.1029/2010tc002697

Müller, T., Koepke, J., Garbe-Schönberg, C. D., Dietrich, M., Bauer, U., & Wolff, P. E. (2017). Anatomy of a frozen axial melt lens from a fast-spreading paleo-ridge (Wadi Gideah, Oman ophiolite). *Lithos*, *272–273*, 31–45. https://doi.org/10.1016/j.lithos.2016.11.022

Natland, J. H., & Dick, H. J. B. (1996). Melt migration through high-level gabbroic cumulates of the East Pacific Rise at Hess deep: The origin of magma lenses and the deep crustal structure of fast-spreading ridges. *Proceedings of the Ocean Distillation Program, Scientific Results*, *147*, 21–58. https://doi.org/10.2973/odp.proc.sr.147.002.1996

Natland, J. H., & Dick, H. J. B. (2009). Paired melt lenses at the East Pacific Rise and the pattern of melt flow through the gabbroic layer at a fast-spreading ridge. *Lithos*, *112*(1–2), 73–86. https://doi.org/10.1016/j.lithos.2009.06.017

Nedimovic, M. R., Carbotte, S. M., Harding, A. J., Detrick, R. S., Canales, J. P., Diebold, J. B., et al. (2005). Frozen magma lenses below the oceanic crust. *Nature*, *436*, 1149–1152

Nicolas, A., & Boudier, F. (2000). *Large mantle upwellings and related variations in crustal thickness in the Oman ophiolite* (Vol. 349, pp. 67–73). Geological Society of America Special Paper. https://doi.org/10.1130/0-8137-2349-3.67

Nicolas, A., Boudier, F., & France, L. (2009). Subsidence in magma chamber and the development of magmatic foliation in Oman ophiolite gabbros. *Earth and Planetary Science Letters*, *284*, 76–87. https://doi.org/10.1016/j.epsl.2009.04.012

Nicolas, A., Boudier, F., Ildefonse, B., & Ball, E. (2000). Accretion of Oman and United Arab Emirates ophiolite - Discussion of a new structural map. *Marine Geophysical Researches*, *21*(3–4), 147–179. https://doi.org/10.1023/a:1026769727917

Nicolas, A., Mainprice, D., & Boudier, F. (2003). High temperature seawater circulation throughout crust of oceanic ridges. A model derived from the Oman ophiolite. *Journal of Geophysical Research*, *108*. https://doi.org/10.1029/2002jb002094

Pallister, J. S., & Hopson, C. A. (1981). Samail Ophiolite plutonic suite: Field relations, phase variation, cryptic variation and layering, and a model of a spreading ridge magma chamber. *Journal of Geophysical Research: Solid Earth*, *86*(B4), 2593–2644. https://doi.org/10.1029/JB086iB04p02593

Pallister, J. S., & Knight, R. J. (1981). Rare Earth element geochemistry of the Samail ophiolite near Ibra, Oman. *Journal of Geophysical Research*, *86*, 2673–2697. https://doi.org/10.1029/jb086ib04p02673

Perk, N. W., Coogan, L. A., Karson, J. A., Klein, E. M., & Hanna, H. D. (2007). Petrology and geochemistry of primitive lower oceanic crust from Pito deep: Implications for the accretion of the lower crust at the southern East Pacific Rise. *Contributions to Mineralogy and Petrology*, *154*(5), 575–590. https://doi.org/10.1007/s00410-007-0210-z

Peters, T., Blechschmidt, I., Krystyn, L., Dumitrica, P., Mercolli, I., El Amin, O., & Al Towaya, A. (2005). *Geological map of Ibra (1:100,000). Sultanate of Oman, Ministry of Commerce and industry, sheet NF 40-48 A*.

Pouchou, J. L., & Pichoir, F. (1991). Quantitative analysis of homogeneous or stratified microvolumes applying the model "PAP. In K. F. J. Heinrich, & D. E. Newbury (Eds.), *Electron probe quantification* (pp. 31–75). Plenum Press. https://doi.org/10.1007/978-1-4899-2617-3_4

Quick, J. E., & Denlinger, R. P. (1993). Ductile deformation and the origin of layered gabbro in ophiolites. *Journal of Geophysical Research*, *98*(B8), 14015–14027. https://doi.org/10.1029/93jb00698

Rioux, M., Bowring, S., Kelemen, P., Gordon, S., Dudas, F., & Miller, R. (2012). Rapid crustal accretion and magma assimilation in the Oman-UAE ophiolite: High precision U-Pb zircon geochronology of the gabbroic crust. *Journal of Geophysical Research*, *117*. https://doi.org/10.1029/2012jb009273

Rioux, M., Bowring, S., Kelemen, P., Gordon, S., Miller, R., & Dudas, F. (2013). Tectonic development of the Samail ophiolite: High-precision U-Pb zircon geochronology and Sm-Nd isotopic constraints on crustal growth and emplacement. *Journal of Geophysical Research: Solid Earth*, *118*(5), 2085–2101. https://doi.org/10.1002/jgrb.50139

Schmitt, A. K., Perfit, M. R., Rubin, K. H., Stockli, D. F., Smith, M. C., Cotsonika, L. A., et al. (2011). Rapid cooling rates at an active mid-ocean ridge from zircon thermochronology. *Earth and Planetary Science Letters*, *302*(3–4), 349–358. https://doi.org/10.1016/j.epsl.2010.12.022

Sun, C., & Lissenberg, C. J. (2018). Formation of fast-spreading lower oceanic crust as revealed by a new Mg–REE coupled geospeedometer. *Earth and Planetary Science Letters*, *487*, 165–178. https://doi.org/10.1016/j.epsl.2018.01.032

Teagle, D., Ildefonse, B., Blum, P. & the Expedition 335 Scientists. (2012). Expedition 335; summary. *Proceedings IODP*, *335*. https://doi.org/10.2204/iodp.proc.335.101.2012

Theissen-Krah, S., Iyer, K., Rüpke, L. H., & Morgan, J. P. (2011). Coupled mechanical and hydrothermal modeling of crustal accretion at intermediate to fast spreading ridges. *Earth and Planetary Science Letters*, *311*(3), 275–286. https://doi.org/10.1016/j.epsl.2011.09.018

Theissen-Krah, S., Rüpke, L. H., & Hasenclever, J. (2016). Modes of crustal accretion and their implications for hydrothermal circulation. *Geophysical Research Letters*, *43*(3), 1124–1131. https://doi.org/10.1002/2015GL067335

VanTongeren, J. A., Hirth, G., & Kelemen, P. B. (2015). Constraints on the accretion of the gabbroic lower oceanic crust from plagioclase lattice preferred orientation in the Samail ophiolite. *Earth and Planetary Science Letters*, *427*, 249–261. https://doi.org/10.1016/j.epsl.2015.07.001

VanTongeren, J. A., Kelemen, P. B., Garrido, C. J., Godard, M., Hanghoj, K., Braun, M., & Pearce, J. A. (2021). The composition of the lower oceanic crust in the Wadi Khafifah section of the southern Samail (Oman) ophiolite. *Journal of Geophysical Research: Solid Earth*, *126*, e2021JB021986. https://doi.org/10.1029/2021JB021986

VanTongeren, J. A., Kelemen, P. B., & Hanghoj, K. (2008). Cooling rates in the lower crust of the Oman ophiolite: Ca in olivine, revisited. *Earth and Planetary Science Letters*, *267*, 69–82. https://doi.org/10.1016/j.epsl.2007.11.034

Vera, E. E., Mutter, J. C., Buhl, P., Orcutt, J. A., Harding, A. J., Kappus, M. E., et al. (1990). The structure of 0-my to 0.2-my old oceanic crust at 9° N on the East Pacific Rise from expanded spread profiles. *Journal of Geophysical Research*, *95*(B10), 15529–15556. https://doi.org/10.1029/JB095iB10p15529

Wanless, V. D., & Shaw, A. M. (2012). Lower crustal crystallization and melt evolution at mid-ocean ridges. *Nature Geoscience*, *5*(9), 651–655. https://doi.org/10.1038/ngeo1552

Wilson, D. S., Teagle, D. A. H., Alt, J. C., Banerjee, N. R., Umino, S., Miyashita, S., et al. (2006). Drilling to gabbro in intact ocean crust. *Science*, *312*, 1016–1020. https://doi.org/10.1126/science.1126090

Wolff, P. E., Koepke, J., & Feig, S. T. (2013). The reaction mechanism of fluid-induced partial melting of gabbro in the oceanic crust. *European Journal of Mineralogy*, *25*(3), 279–298. https://doi.org/10.1127/0935-1221/2013/0025-2314

Zhang, C., Koepke, J., Kirchner, C., Goetze, N., & Behrens, H. (2014). Rapid hydrothermal cooling above the axial melt lens at fast-spreading mid-ocean ridge. *Scientific Reports*, *4*, 6342. https://doi.org/10.1038/srep06342

Zihlmann, B., Müller, S., Coggon, R. M., Koepke, J., Garbe-Schönberg, D., & Teagle, D. A. H. (2018). Hydrothermal fault zones in the lower oceanic crust: An example from Wadi Gideah, Samail ophiolite, Oman. *Lithos*, *323*, 103–124. https://doi.org/10.1016/j.lithos.2018.09.008